ACOUSTICS IN THE KLEBANOFF–SARIC WIND TUNNEL: BACKGROUND IDENTIFICATION, FORCING, AND ACTIVE CONTROL

A Thesis

by

MATTHEW SCOTT KUESTER

Submitted to the Office of Graduate Studies of
Texas A&M University
in partial fulfillment of the requirements for the degree of

MASTER OF SCIENCE

May 2012

Major Subject: Aerospace Engineering

Acoustics in the Klebanoff–Saric Wind Tunnel: Background Identification, Forcing, and Active Control

ACOUSTICS IN THE KLEBANOFF–SARIC WIND TUNNEL: BACKGROUND IDENTIFICATION, FORCING, AND ACTIVE CONTROL

A Thesis

by

MATTHEW SCOTT KUESTER

Submitted to the Office of Graduate Studies of
Texas A&M University
in partial fulfillment of the requirements for the degree of

MASTER OF SCIENCE

Approved by:

Chair of Committee,	Edward White
Committee Members,	William Saric
	Yong-Joe Kim
Head of Department,	Dimitris Lagoudas

May 2012

Major Subject: Aerospace Engineering

ABSTRACT

Acoustics in the Klebanoff–Saric Wind Tunnel: Background Identification, Forcing, and Active Control. (May 2012)

Matthew Scott Kuester, B.S., Texas A&M University

Chair of Advisory Committee: Dr. Edward White

Low disturbance wind tunnels, such as the Klebanoff–Saric Wind Tunnel (KSWT), offer an ideal environment to study boundary layer transition. In particular, the leading-edge receptivity of sound can be measured by creating acoustic disturbances that interact with the leading edge of a model to create Tollmien–Schlichting waves. The magnitude and composition (sound, turbulence) of the background disturbances can affect these experiments, so the background disturbances should be minimized and documented thoroughly.

The purpose of this thesis is to document the background acoustic signature of the KSWT and describe infrastructure upgrades for acoustic receptivity experiments. The measurements presented in this thesis will support future receptivity measurements in the KSWT.

Microphone measurements revealed several important acoustic features in the tunnel. Cross correlations showed that two sources of low-frequency unsteadiness (the extended diffuser and corner two) create large pressure fluctuations that dominate the pressure spectrum. Directional separation of waves in the test section revealed that motor

and blade passing noise travels primarily upstream into the test section. Finally, the acoustic treatments in the plenum are effective at removing sound from the tunnel.

A wall of speakers was installed in the plenum to enable acoustic receptivity experiments. The speakers create both the primary downstream traveling waves and reflected upstream traveling waves in the test section. An adaptive closed loop control system was installed to reduce the amplitude of the reflected waves during acoustic forcing. Although the performance of the control system is frequency dependent, the technique was implemented successfully. The reduction in the diffuser reflection will increase the quality of future acoustic receptivity experiments in the KSWT.

ACKNOWLEDGEMENTS

I would like to first acknowledge the support of NASA and AFOSR through AFOSR grant FA9550-09-1-0341. I would also like to acknowledge the NASA/ASEE Aeronautics Scholarship program for support through a graduate fellowship.

Thank you to my committee chair, Dr. White, and my committee members, Dr. Saric and Dr. Kim, for their guidance and support throughout the course of this research. I want to especially acknowledge Dr. Saric for the use of the Klebanoff–Saric Wind Tunnel and his sound receptivity experiments performed at Arizona State that led to the motivation for this thesis.

I would also like thank my friends and colleagues at the Flight Research Laboratory, the Oran W. Nicks Low Speed Wind Tunnel, and the Klebanoff–Saric Wind Tunnel. In particular, special thanks to Rob Downs, Lauren Hunt, David West, Jason Monschke, Bob Long, Brian Crawford, and Nicole Sharp, who all helped with various aspects of this work.

I would like to thank my parents for their continuous love and support. Finally, I would like to thank my wife for being with me for every step of the process; this thesis would not have been possible without her encouragement and love.

TABLE OF CONTENTS

Page

LIST OF FIGURES

FIGURE Page

FIGURE Page

LIST OF TABLES

TABLE Page

1. INTRODUCTION AND BACKGROUND: THE ROLE OF WIND TUNNEL ACOUSTICS IN RECEPTIVITY EXPERIMENTS

Understanding and controlling boundary layer transition from laminar to turbulent flow is critical for numerous aerodynamic applications. For example, the reduction in skin friction drag for laminar flow compared to turbulent flow could increase the range and fuel efficiency of commercial airliners. In spite of its importance, transition is still not fully understood.

Boundary layer transition is an initial value problem wherein sound, freestream turbulence and roughness create boundary layer fluctuations. The process of how environmental disturbance become boundary layer fluctuations, called receptivity, is important because it sets the initial amplitudes of disturbances that grow and eventually lead to turbulence. Receptivity has been studied for over 40 years, but remains poorly understood. Understanding receptivity will enable more reliable predictions of transition using theoretical and numerical models.

Carefully planned experiments in low disturbance environments broaden our understanding of receptivity. The effect of environmental disturbances on boundary layer transition can be seen in Figure 1 (from Morkovin et al. 1994) which shows the boundary layer transition roadmap. As the amplitude of environmental disturbances increases, transition occurs through different physical mechanisms. Testing in a low disturbance environment is essential for studying the mechanics of boundary layer

---

This thesis follows the style of Experiments in Fluids.

receptivity, stability and transition through the paths on the left side of the roadmap.

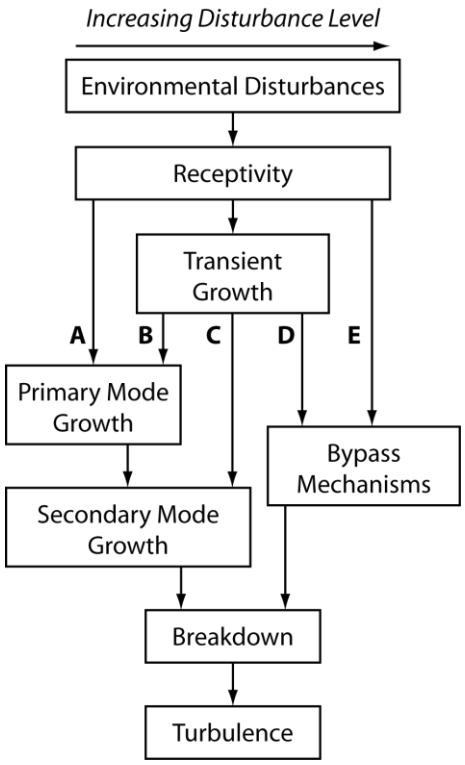

Figure 1. Boundary layer transition roadmap (Morkovin et al. 1994)

Once a low disturbance environment has been established, the effect of particular disturbances can then be studied by adding larger, controlled disturbances to the base flow and studying their receptivity. Figure 2 shows the neutral stability curve of a Blasius boundary layer; the curve shows the Reynolds numbers where disturbances with a certain frequency are spatially unstable. Disturbances with known frequencies can be inserted into an experiment to disturb the boundary layer and trigger these unsteady modes (in this case, Tollmien–Schlichting (T-S) waves). Measuring both the

environmental and boundary layer disturbances yields the receptivity of the environmental disturbance.

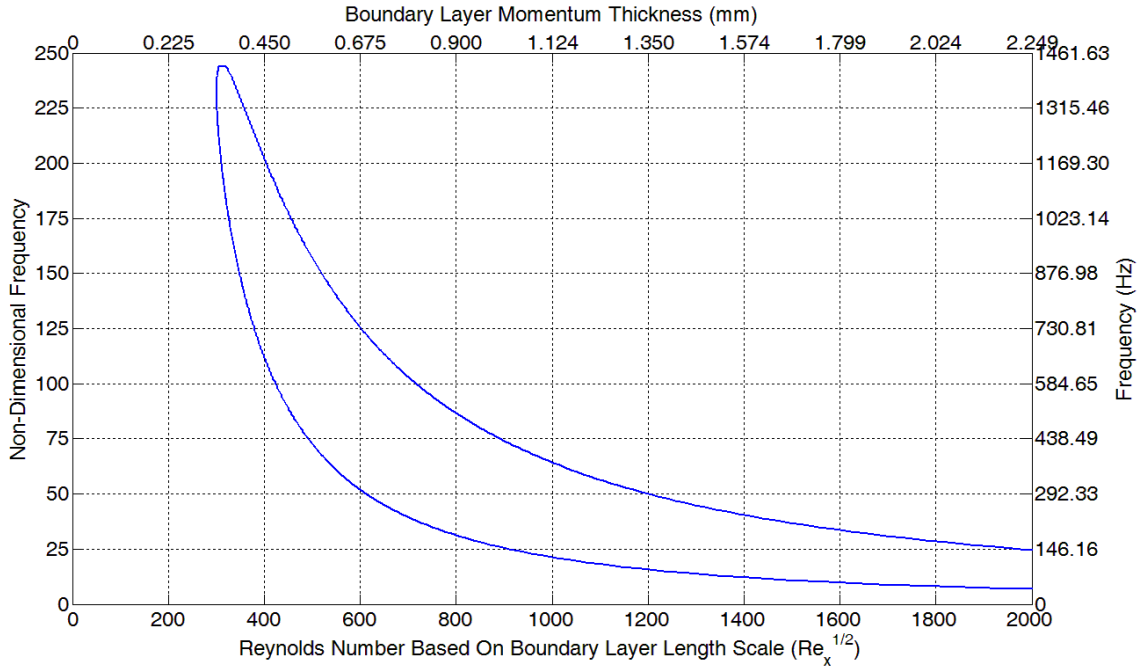

Figure 2. Neutral stability curve of the Blasius boundary layer for U_∞ = 24 m/s, ν = 15.68×10^{-6} m^2/s

This thesis documents the preparation of the Klebanoff–Saric Wind Tunnel (KSWT) facility for experiments in boundary layer receptivity to freestream sound. Previous work (Hunt et al. 2010) documented turbulence levels in the KSWT, but this thesis thoroughly documents the background sound field inside the test section. Once the background sound levels were documented, infrastructure upgrades were installed to the wind tunnel to enable acoustic receptivity experiments.

1.1 The Role of Sound in Boundary Layer Transition

As discussed in the introduction, receptivity is the mechanism in which environmental disturbances enter the boundary layer and set the initial conditions for boundary layer disturbances. Sound and turbulence play different roles in transition; Kendall (1991) showed that vortical disturbances contribute to the 3-D aspects of breakdown while theory, experiments and direct numerical simulation (DNS) have shown that sound is the main receptivity mechanism for T-S waves. Because this thesis focuses on acoustics rather than turbulence, sound receptivity will be the focus of this section.

Early theoretical work formed the foundation of sound receptivity experiments. Goldstein (1983) utilized triple deck theory and the unsteady boundary layer equations to show that the interaction of freestream disturbances with large streamwise gradients at the leading edge creates unstable waves that match the behavior of T-S waves as they travel downstream. Further theoretical studies focused on the interaction of sound with non-localized surface irregularities (Crouch 1992a) and localized regions such as areas of strong streamwise gradients (Kerschen 1990) or localized roughness (Crouch 1992b). These studies showed that a T-S wave is created through the interaction of disturbance modes near the surface; this interaction provides the mechanism to turn the long-wavelength acoustic wave into the short-wavelength boundary layer T-S wave.

Experiments and DNS have built upon the early theoretical receptivity framework. Experiments were designed to study a specific receptivity mechanism (localized roughness, distributed roughness, and the leading edge). Because most

aerodynamic shapes have a leading edge, leading edge receptivity has been a focus of many receptivity experiments. Some of these experiments, including matching DNS studies, will be discussed later in this section.

Despite the research in the field of sound receptivity, more experimental studies are required. For example, parabolic leading edge receptivity to sound has been addressed by theory (Hammerton & Kerschen 1996) and DNS (Haddad et al 2005), but no published experiment has ever confirmed these results. Continued acoustic receptivity experiments will provide a means of comparison for theoretical studies and broaden our understanding of receptivity.

1.2 The Need for Low-Disturbance Wind Tunnels

Wind tunnels provide a controlled means to make detailed stability and transition measurements, but wind tunnels also introduce freestream disturbances that are not typically found in flight. These disturbances must be minimized to create a test environment as close to the flight environment as possible.

Pressure waves found in wind tunnels can be caused by several sources. Unsteady flow, caused by flow separation in diffusers and corners, has typical frequencies below the audible range. Tonal disturbances, such as blade passing and motor noise, have a consistent phase and are often in the frequency range of unstable T-S waves. Higher frequency noise is created in the wakes of turning vanes, splitter plates, and the model. All three types of pressure fluctuations can adversely affect the quality of a boundary layer transition experiment.

Saric and Reshotko (1998) give criteria for turbulence intensities and static pressure fluctuation levels in wind tunnels used for boundary layer stability and transition experiments. Although some tunnels such as aeroacoustic tunnels used by car manufacturers have low noise levels, these tunnels do not have the low turbulence characteristics required for sensitive experiments (Duell et al. 2002). Wind tunnels used in boundary layer transition experiments should have low disturbance levels with documented frequency and amplitude content. Documentation of background disturbances will help build correlations between different disturbances and transition behavior. Section 3 of this thesis is devoted to documentation of background noise levels in the Klebanoff–Saric Wind Tunnel (KSWT) at Texas A&M University.

1.3 Previous Experiments Measuring Leading Edge Receptivity

Initial attempts to make leading edge acoustic receptivity experiments were unsuccessful. Nishioka & Morkovin (1986) describe the reasons why these experiments were biased by environmental conditions. Experiments at Arizona State University (ASU) in the 1990s were some of the first experiments that studied leading edge receptivity without these biases.

Early experiments at ASU focused on sound receptivity of a flat plate with an elliptic leading edge. Speakers created sound that traveled downstream and interacted with the leading edge to create T-S waves. The T-S waves were then measured using a hotwire inside the boundary layer further downstream. With continuous acoustic forcing, a measurement inside the boundary layer will be a superposition of Stokes waves and T-S waves with the same frequency. Saric et al. (1995) separated the waves by making

several measurements spanning one wavelength of the T-S wave at a constant height in the boundary layer. The separation of scales between the Stokes wave and the T-S wave enabled the two waves to be measured separately when plotted in the complex plane.

Although this technique allows T-S wave amplitudes to be measured, it has several disadvantages. In order to get a well-resolved spiral in the complex plane, measurements must be taken at 15-30 streamwise locations. The process must then be repeated for each wall-normal distance. In order to obtain one receptivity coefficient, complete wall-normal boundary layer scans must be performed at several streamwise locations. The amount of measurements makes the spiral technique tedious when performing multiple sets of receptivity measurements.

Another issue with this technique was addressed by Saric et al (1999). They concluded from measurements made by Krutckoff (1996) that continuous acoustic forcing was causing a wake resonance. The wake resonance was in turn creating an asymmetric oscillation in the test section. Velocity disturbances transverse to the leading edge were then amplifying the T-S waves at frequencies where wake resonance was occurring. This theory explained the frequency selection effect noticed by Saric et al. (1999).

A third challenge with continuous forcing is standing waves in the test section created by acoustic reflections. The speakers in the plenum emit a continuous sound wave that travels downstream through the test section and reaches the first stage diffuser. The change in area from the diffuser creates reflected waves that travel upstream. The interaction between the main, downstream traveling waves and the reflected, upstream

waves can create a standing wave pattern in the test section. The standing wave can modulate the amplitude of the acoustic forcing at the leading edge through constructive/destructive interference. The receptivity of upstream and downstream traveling waves is different (Heinrich 1989), so any receptivity measurements will be a combination of T-S waves created by upstream and downstream traveling acoustic waves.

Later experiments at ASU (Saric and White 1998, White and Saric 2000) used a pulsed sound technique to study leading edge receptivity. In this technique, short bursts of sound travel downstream and interact with the leading edge to create T-S waves. Inside the boundary layer, the Stokes waves created by the sound burst travel downstream at the speed of sound, while the T-S waves travel downstream at a fraction of the freestream speed. As the T-S waves travel downstream, the forcing sound wave spreads and dissipates throughout the tunnel. The T-S waves are then measured inside the boundary layer using a hotwire and are conditionally sampled such that the Stokes waves do not affect the experiment.

By using sound pulses and conditional sampling, White and Saric removed the wake resonance complication that arose in earlier experiments from continuous acoustic forcing. The conditionally sampled T-S waves were then analyzed in the frequency domain. A second hotwire in the freestream at the leading edge measured the freestream sound wave, and the receptivity coefficient was calculated in the frequency domain. These receptivity coefficients closely matched the DNS results of Fuciarelli et al. (2000).

One of the largest drawbacks of this technique is the frequency resolution of the receptivity coefficients. The frequency resolution is directly proportional to the signal time length, and the signal time length is limited due to the conditional sampling of the pulsed waves. Another drawback of this technique is the ensemble averaging required to obtain an accurate receptivity coefficient. The real and imaginary components of the receptivity coefficients are ensemble averaged to remove the effect of uncorrelated disturbances. Saric et al (1999) states that 200-800 ensemble averages are required for the receptivity coefficient to converge. A measurement technique that can directly measure T-S wave amplitude without requiring ensemble averaging would expedite leading edge receptivity measurements.

Resolving issues associated with continuous acoustic forcing will enable new receptivity measurement techniques such as modal decomposition of the Orr-Sommerfeld equation. Wiegel and Wlezien (1993) used a secondary loudspeaker downstream of the test section to eliminate standing waves in the test section during continuous acoustic forcing. Removing standing waves was important for their experiment because they were studying distributed receptivity and required constant amplitude forcing throughout the entire test section. It is unclear whether the global circulation effect measured by Krutckoff (1996) is caused by the downstream traveling sound wave with consistent phase or the standing wave created by the upstream traveling sound. If the upstream traveling reflection from acoustic forcing is removed, the frequency selection effect may be eliminated. This would enable experimental techniques that use continuous acoustic forcing to measure acoustic receptivity.

This thesis documents the acoustic features of the KSWT in preparation for acoustic receptivity experiments. Section 2 describes the KSWT facility and experimental techniques used in this thesis. Section 3 focuses on the background noise levels in the KSWT, while Section 4 focuses on the effect of the tunnel acoustic treatments on the background noise levels. Section 5 discusses the installation of a speaker wall to provide acoustic forcing for experiments. Finally, Section 6 describes the implementation of a closed loop control system that reduces the diffuser reflection created from acoustic forcing; this control system will enable new techniques using continuous acoustic forcing to measure leading edge acoustic receptivity.

2. THE KLEBANOFF–SARIC WIND TUNNEL AND EXPERIMENTAL TECHNIQUES

Section 1 outlined the need for low disturbance wind tunnels to study boundary layer transition. The KSWT at Texas A&M University is a low speed, low disturbance wind tunnel designed for boundary layer stability and transition experiments. The KSWT, which was used in sound receptivity experiments at ASU (Saric et al. 1995, Saric & White 1998, Saric et al. 1999, White et al. 2000) under the name ASU Unsteady Wind Tunnel, was relocated to Texas A&M in 2005. The tunnel was reconstructed at Texas A&M with modifications to improve flow quality and decrease flow disturbance levels. Hunt et al. (2010) describes the KSWT in detail, presents freestream turbulence measurements at several points in the test section, and provides preliminary information about noise levels in the tunnel.

This section starts by describing the KSWT and the features that make it a low disturbance wind tunnel. Information about the instrumentation and sound detection equipment used in the KSWT is also provided. The section concludes with an outline of experimental techniques used in this thesis.

2.1 Wind Tunnel Configuration

The KSWT is a closed-loop, low disturbance wind tunnel designed to study boundary layer transition in low speed flows. The air speed in the test section can reach 31 m/s and can be controlled accurately within 0.1 m/s. A tunnel overhead view can be seen in Figure 3.

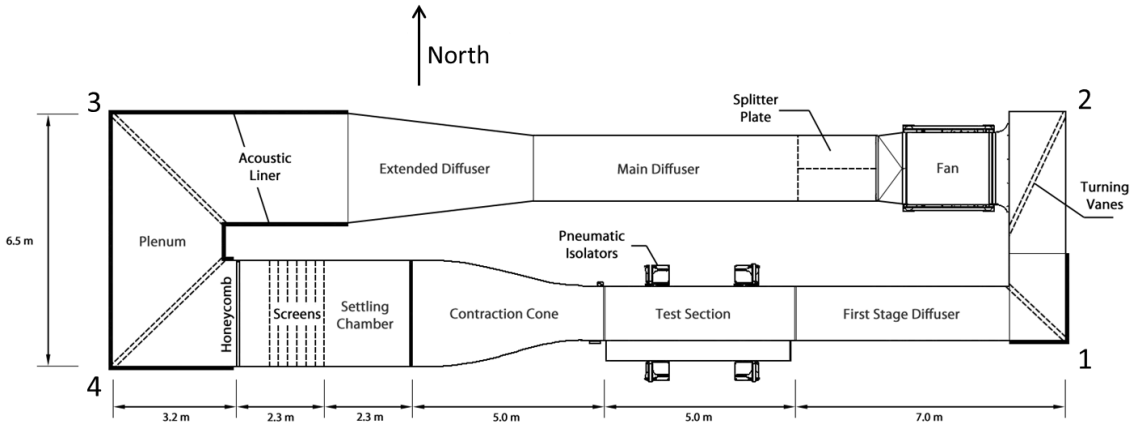

Figure 3. Top view of the Klebanoff–Saric Wind Tunnel

2.1.1 *Test Section*

The tunnel has two interchangeable test sections. Each is 4.9 m long and has a 1.4 by 1.4 m square cross section at the upstream end. The test section diverges slightly in the vertical direction to account for boundary layer growth on the tunnel walls; the cross section at the downstream end of the test section is 1.41 m by 1.4 m. Since reconstruction of the tunnel at Texas A&M, the test section holding a swept wing experiment has been installed in the tunnel. The swept wing test section rests on pneumatic isolating units (Fabreeka® Precision-Aire™ PAL 21) that isolate the test section from building vibrations. The pneumatic isolators remove structural vibrations that induce velocity and acceleration biases in hotwire and microphone measurements. To avoid additional vibration transfer, the test section is connected to the rest of the tunnel with flexible couplings. The test sections also have interchangeable windows; one of the windows offers a large viewing area while another supports a three dimensional traverse for detailed hotwire scans.

2.1.2 *Fan and Motor*

The tunnel is powered by an Emerson Industrial Controls 150 horsepower, variable speed 1750 maximum RPM direct current motor. The motor is connected to a Howden Buffalo nine-bladed, 6’ diameter, adjustable-pitch axial fan through a belt drive system. With the fan installed, the maximum RPM is 1300. Eleven stators downstream of the fan remove fan-induced flow swirl. A nacelle and fairings surround the power transmission cartridge and drive belt, respectively. The fan sits inside of a metal housing that is not rigidly connected to any other part of the tunnel; flexible rubber couplings connect the fan housing at both the upstream and downstream ends. The fan housing is supported by the same steel structure that supports the motor. The motor sits directly underneath the fan housing, and the entire structure is surrounded by a plywood enclosure that is lined on the interior with egg crate acoustic foam. This enclosure reduces the amount of motor noise that could contaminate experiments.

At ASU, the motor was connected to the fan in a direct-drive configuration. Moving the motor outside of the tunnel reduced the amount of motor noise in the flow. The change from a direct drive system to a belt drive system also improved experimental control; during operation, the motor releases hot, turbulent jets of gas that affected experiments. With the new configuration, the motor can be cooled effectively without increasing the tunnel temperature.

In the current motor configuration, the maximum motor frequency is 21.7 Hz. The nine-blade fan produces blade passing noise at nine times the motor frequency with the maximum blade passing frequency (BPF) at 195 Hz. The tunnel is controlled by

adjusting motor RPM, so motor and blade passing frequencies change with test section speed and blockage.

2.1.3 *Diffusers and Contractions*

The cross sectional area of the KSWT increases at three locations around its circuit: the main diffuser, the extended diffuser, and the first stage diffuser (see Figure 3). The main diffuser and the extended diffuser have expansion angles of 12 degrees, while the first stage diffuser has an expansion angle of 10 degrees. Each diffuser has a full length splitter plate that halves the expansion and helps prevent unsteady separation bubbles. Two screens located in the main diffuser also promote attached flow.

The contraction cone, located directly upstream of the test section, reduces the cross-sectional area of the tunnel by a factor of 5.33 and has an L/D of 1.25. The contraction is a fifth-degree polynomial shape with zero slope and zero curvature at both the upstream and downstream ends. The contraction cone is designed to prevent a separation bubble that can cause low frequency pressure oscillations.

2.1.4 *Honeycomb and Screens*

Several components along the test leg of the tunnel are specifically designed to lower turbulence levels. A sheet of aluminum honeycomb is located directly downstream of corner four. The honeycomb is made of hexagonal cells that are three inches long and 0.25 inch maximum width. The honeycomb is designed to straighten the flow and reduce large turbulence scales.

Seven tensioned screens, placed downstream of the honeycomb, promote mean flow uniformity and reduce turbulence scales. Each screen is made of 0.0065 inch

diameter stainless steel wire arranged in a 30 wire/inch mesh. The screens are each separated by nine inches to allow spatial decay of disturbances between each screen. The first three screens are butt welded while the final four are seamless.

2.1.5 *Control and Data Acquisition*

All measurements, including static pressure, dynamic pressure, tunnel air temperature and microphone measurements are collected using three National Instruments USB data acquisition boards (Model USB-6211). Using three boards provides 24 differential analog inputs (-10 V to +10 V maximum range) for tunnel control and measurements. One of the boards is exclusively used to measure tunnel conditions (static pressure, dynamic pressure and temperature), while the other two boards are used for acquiring measurements. All aspects of tunnel control (motor rpm, data acquisition and traverse movement) are integrated in an in-house C++ routine created by Rob Downs and Brian Crawford. The control program uses static pressure, dynamic pressure and temperature information to set the motor RPM to maintain constant velocity, Reynolds number, or fan speed. The accuracy of the pressure transducers and RTD allow velocity to be controlled to within ± 0.1 m/s.

2.1.6 *Acoustic Treatments*

During the tunnel's reconstruction at Texas A&M, 37 Modex™ Broadband Panels from RPG Diffuser Systems were mounted in the plenum on the ceilings, walls, and floors. These panels are designed to eliminate sound in 50 – 5000 Hz range. The main component of the panel is a thin steel plate backed with a sound absorbing spring material. Vibration and bending of the plate caused by acoustic pressure fluctuations are

damped by the absorbing material. The plate and spring material are encased in a perforated metal casing that is only 4.25 inches deep; the small thickness makes these panels ideal for the space-constrained tunnel environment. The panels are placed near intersections of walls where the pressure fluctuations have the highest magnitude. The layout of the panels in the plenum can be seen in Figure 4.

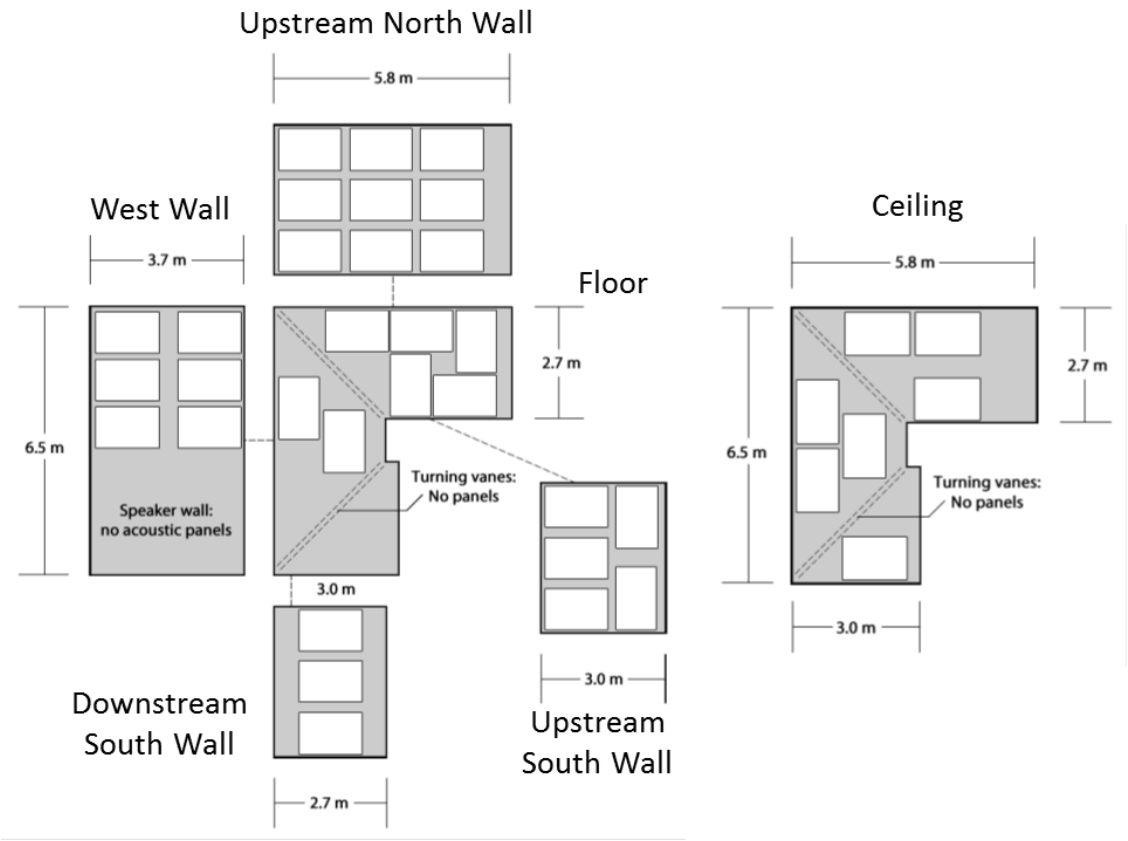

Figure 4. Layout of broadband acoustic panels on plenum floor, walls, and ceiling

Dense, 4.25 inch thick open cell acoustic foam from dB engineering was installed around the acoustic panels. The thickness limits the frequency absorption range

of the foam to greater than 150 Hz. Although lower frequencies are more important for receptivity experiments, the foam reduces overall noise while creating a flat tunnel wall between the panels and the foam.

Three acoustic panels and additional foam (not shown in Figure 4) were installed in corner one. These treatments serve two purposes; first, they help remove upstream traveling fan and motor noise. Secondly, the acoustic treatments help remove downstream traveling noise from the test section. In particular, noise generated in the wake of the model reflect and travel upstream back into the test section.

2.2 Sound Measurement Instrumentation

All sound measurements are made using PCB ½" random incidence, pre-polarized condenser microphones (Model 377B20). The microphones have a linear response (± 2 dB) between 3.15 Hz and 12.5 kHz and a dynamic range of 15 dB (A) to 146 dB (A). The microphones measure static pressure fluctuations in the tunnel.

The grid cap on each of the microphones was replaced with a nose cone (PCB 079B21) for in-flow measurements. The nose cone is specifically designed to remove aerodynamic noise from microphone measurements. According to correction curves provided by PCB Piezotronics, the nose cone does not alter the microphone response (± 1 dB) up to 5 kHz. Tests performed in the KSWT showed that the nose cone can more effectively remove wind-induced noise than the grid cap or a 4" diameter wind screen.

The microphones are connected to a preamplifier (PCB Model 426E01) which is then connected to a signal conditioner (PCB Model 482A22). The signal conditioner provides the current excitation (2-20 mA) required for the pre-polarized microphones.

Finally, the microphone signals are filtered and amplified using a Stewart/Kemo VBF44 analog filter. Each filter has two band-pass filters that can be tuned for cutoff ranges between 1 Hz and 255 kHz. The typical band-pass setting for microphone measurements is 1 Hz – 5 kHz. A +20 dB gain is applied to each microphone signal to utilize the full resolution of the data acquisition system.

2.3 Measurement Techniques

Several techniques are used throughout this thesis to analyze microphone data and gain information about wind tunnel acoustics. Microphone calibrations ensure microphone measurements are accurate. Sound pressure level calculations and acoustic spectra show the magnitude and frequencies of sound in the wind tunnel. Finally, single-direction sound detection separates the acoustic field in the wind tunnel into upstream and downstream traveling waves.

2.3.1 *Microphone Calibration*

All microphones used in the KSWT were calibrated daily using a PCB/Larson Davis CAL250 acoustic calibrator. The calibrator outputs a 114.01 dB sound wave at 251.2 Hz inside the calibration chamber. Each microphone is placed inside the calibration chamber, and the output is measured through the data acquisition system. A calibration constant can then be calculated for each microphone from the acquired data. Although the calibration constants did not show considerable change from day to day, the calibration sequence ensured that all components of the microphone system (microphone, pre-amplifier, cable, signal conditioner, and data acquisition) were functioning correctly.

2.3.2 *Sound Pressure Level*

The amplitude of pressure fluctuations is expressed as the sound pressure level (SPL). The SPL is a log scale, expressed in decibels (dB), that compares a root mean square (rms) pressure fluctuation to a reference pressure, $p_{ref} = 20x10^{-6}$ Pa. The SPL can be computed using Equation (1).

$$SPL = 10\log_{10}\left(\left(\frac{p_{rms}}{p_{ref}}\right)^2\right) \quad (1)$$

The SPL represents the total pressure fluctuation level with contributions from all frequencies. The distribution of power among the different frequencies can be found by calculating the power spectral density (PSD). The power spectral density is calculated using Welch's method (Welch 1967). This method averages periodograms of overlapping, windowed data segments. The PSD shows how the power of the signal is distributed over the frequency range from 0 Hz to the Nyquist frequency.

The PSD is then normalized such that

$$p_{rms}^2 = \sum_{n=0}^{N} PSD(f_n) \quad (2)$$

After normalization, each component of the PSD represents the power of pressure fluctuations in a certain frequency bin. Finally, the normalized PSD is expressed in a decibel scale as the narrowband SPL, shown in Equation (3).

$$Narrowband\ SPL = 10\log_{10}\left(\frac{PSD}{{p_{ref}}^2}\right) \quad (3)$$

The narrowband SPL gives the sound pressure level for each frequency band of the pressure fluctuation. The standard data acquisition time for microphone

measurements in this thesis is 60 seconds; after splitting each measurement into segments and averaging, the standard Δf for the narrowband SPL is less than 0.04 Hz.

Being able to examine the frequency content of a pressure fluctuation is critical when flow disturbances of different frequencies cause different boundary layer transition behavior, so microphone measurements in this thesis will present the narrowband SPL spectrum as well as the overall SPL for each measurement.

2.3.3 *Cross Correlations*

Cross correlations are used in this thesis to localize the origin of low frequency pressure fluctuations. In a cross correlation, two signals are compared in order to determine how the signals are related. The discrete correlation of two sampled functions is defined by Equation (4) (Press et al. 2007).

$$Corr(a,b)_j = \sum_{m=1}^{N} a_{j+m} b_m \tag{4}$$

The cross correlation, which is a function of the offset j, describes how similar the two signals are when signal a is offset by j points. j can be positive or negative depending on which signals lags behind the other. In this thesis, the cross correlations are normalized such that a perfectly correlated signal has a maximum correlation of one. The normalization is shown in Equation (5).

$$Corr(a,b)_{j,\ normalized} = \frac{Corr(a,b)_j}{\sqrt{Corr(a,a)_0 Corr(b,b)_0}} \tag{5}$$

The cross correlation can be calculated in the frequency domain by performing a Fourier transform on both signals, taking the conjugate of the transformed reference signal, multiplying the transforms together, and taking the inverse Fourier transform.

This formulation, shown in Equation (6), is identical to the cross correlation shown in Equation (4). In Equation (6), A_k and B_k are the Fourier transforms of a and b, respectively.

$$Corr(a,b)_j = ifft(A_k B_k^*) \quad (6)$$

When the cross correlation is calculated in the frequency domain, both signals are padded with zeros to eliminate bleed over effects from one period of the signal to the next.

2.3.4 *Single Direction Sound Detection*

Leading edge receptivity to sound is affected by sound propagation direction, not just magnitude and frequency (Heinrich 1989). In particular, upstream traveling waves are more effective than downstream traveling waves at interacting with the leading edge to create T-S waves. The ability to document wave direction in the test section is a key component of describing the background noise levels in the tunnel.

Splitting the signal into downstream and upstream traveling waves is straightforward if the sound waves are planar. The planar wave cutoff frequency is the lowest frequency a non-planar wave can propagate through a duct without decaying. The planar cutoff frequency in a rectangular duct is $f_c = c/2l$ where c is the speed of sound and l if the largest dimension of the duct.

All sound waves in the test section with a frequency below the cutoff frequency are either planar or are evanescent, decaying waves. By limiting the analysis to frequencies below the cutoff frequency, complications involving non-planar waves can

be avoided. In particular, the known streamwise wavenumber of planar waves can be utilized to separate downstream and upstream traveling waves.

In the separation technique, shown in Figure 5, two microphones are placed a known streamwise distance apart in the streamwise direction. The microphones simultaneously record the pressure field in the duct. The pressure fluctuations measured by the microphones are the sum of downstream traveling waves, g_1, and upstream traveling waves, g_2. The Fourier transforms of these signals are G_1 and G_2. The time delay for propagation between microphones is taken into account by multiplying by the Laplace transform of the delay. The measurements at the two microphones are represented in the frequency domain in Equations (7) and (8).

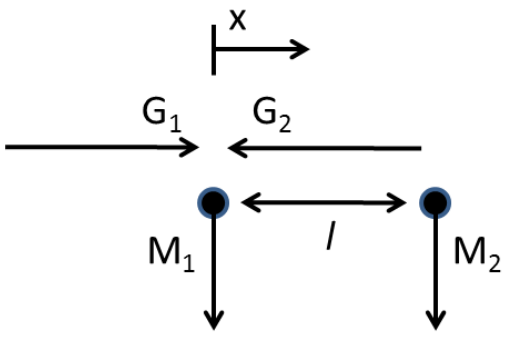

Figure 5. Single direction sensing technique (frequency domain)

$$M_1 = (G_1 + G_2) + \text{c.c.} \tag{7}$$

$$M_2 = \left(G_1 e^{-i(\Delta t)(2\pi f)} + G_2 e^{i(\Delta t)(2\pi f)}\right) + \text{c.c.} \tag{8}$$

Equations (7) and (8) can be solved for G_1 and G_2 as

$$G_1 = \left(\frac{-i}{2\sin\varphi}(M_1 e^{i\varphi} - M_2)\right) + \text{c.c.} \quad (9)$$

$$G_2 = \left(\frac{-i}{2\sin\varphi}(M_2 - M_1 e^{-i\varphi})\right) + \text{c.c.} \quad (10)$$

where $\varphi = (2\pi f)l/c$.

The frequency domain technique described above works well for post processing data, but control applications require directional sensing performed in real time. Manipulating two microphone signals in the frequency domain in real time is not feasible, so this technique needs to be modified for real time applications. In the time domain implementation, shown in Figure 6, the sampling frequency ($f_s = nc/l$, n is a positive integer) is set such that the time delay of sound traveling between the two microphones is equal to a multiple of the time between acquired samples.

Unwanted waves can be eliminated by subtracting the two signals after one of the signals is subjected to an *n* point delay. The measured wave direction can be changed by switching which microphone signal becomes delayed. The resulting signal is a function only of sound waves traveling in one direction; however, the time domain technique does not adjust the amplitude or phase of the signal. Essentially, the time domain technique acts as a filter that removes waves traveling in a certain direction while applying a frequency-dependent transfer function to the remaining signal.

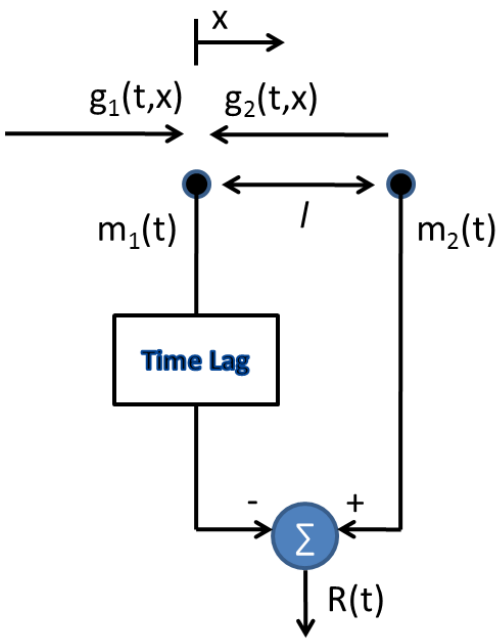

Figure 6. Single direction sensing technique (time domain)

In Equations (9) & (10), the sine term in the denominator illustrates the constraint on the microphone separation. If the two microphones are spaced half a wavelength apart, the resulting output becomes unbounded. Any errors associated with the measurement (phase mismatch between microphones, noise in the signal, round off errors, etc.) become amplified at frequencies where the denominator is small. In particular, this effect is worst at low frequencies and frequencies near the half-wavelength limit. The time domain technique is not constrained by this limitation; however, frequencies near the zeros of the sine term will be naturally filtered rather than magnified.

Both the frequency and time domain techniques have a limitation associated with the assumptions made regarding the applied time lags. For both techniques, sound

traveling in one direction can be completely eliminated by subtracting two different signals. The remaining signals (the numerator in Equations (7) and (8) and R(t) in Figure 6) are actually a combination of two different wave packets traveling in the measurement direction. One of the wave packets has already passed the microphones, while the other wave packet is just arriving at the microphones. If the detected sound consists of single frequencies with constant phase, the two wave packets are related through a wave number relationship. If the sound field consists of pulses or random, non-periodic components, the two wave packets may be unrelated. The resulting decomposed sound field will be a convolution of different wave packets and will not truly represent the upstream and downstream traveling waves. The limitations of this technique will be re-addressed in Sections 3, 4 and 5.

3. TEST SECTION ACOUSTIC SIGNATURE

Section 1 described the need to document the background disturbance levels in wind tunnels. In particular, the irrotational and rotational disturbances should both be documented because they each play a unique role in transition. Hunt et al. (2010) provides thorough documentation of velocity fluctuations and turbulence intensities in the KSWT while this section describes the test section acoustic signature.

3.1 Full Spectrum Acoustic Signature

The acoustic signature of the test section was measured using four microphones. The streamwise location of the microphones is shown in Table 1. Each microphone was placed five inches away from the wall using a ¼" threaded rod as a sting. The microphones were placed at different heights in the test sections to limit noise created in the wake of the microphone stands. Multiple microphones were used for post-processing techniques such as cross correlations and single direction sensing.

Table 1. Test section microphone placement in streamwise direction relative to the test section entrance

	Microphone One	Microphone Two	Microphone Three	Microphone Four
x (m)	0.68	1.90	3.31	4.34

Figure 7 shows the frequency spectrum of measurements taken simultaneously at the four microphone locations. The spectrum shows that the downstream microphones (especially microphone four) are affected by a noise pattern that is not a background

disturbance. Between 30 Hz and 150 Hz, each successive microphone downstream of microphone one has increasing amplitude of broadband noise; Table 2 compares the sound pressure level in the 30 Hz – 150 Hz band for the same measurement. This noise is most likely caused by pressure fluctuations in the wakes of the microphones.

Because microphone one is not affected by the wakes from other microphones, the pressure fluctuations measured at microphone one will be presented for sound pressure levels and pressure spectra. The other microphone signals will be used for single direction sound detection and cross correlations.

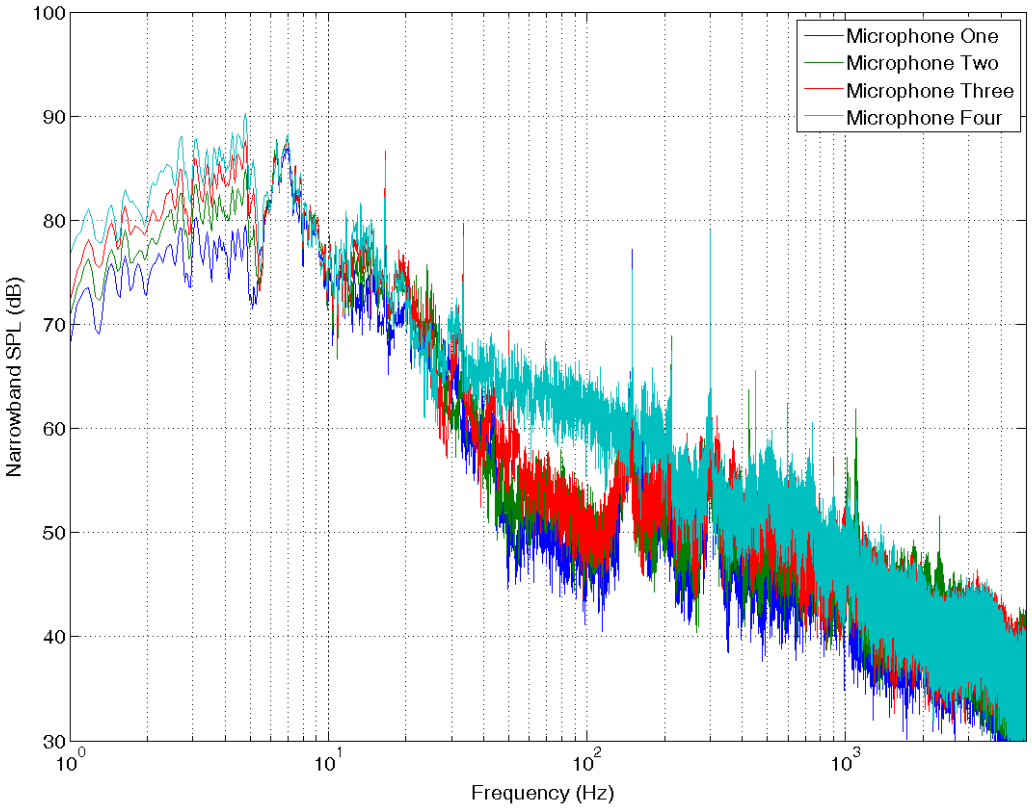

Figure 7. Comparison of microphone spectra for baseline acoustic signature at 1000 RPM

Table 2. Comparison of microphone broadband noise in the 30 Hz - 150 Hz band at 1000 RPM

	Microphone One	Microphone Two	Microphone Three	Microphone Four
30 Hz – 150 Hz Band (dB)	91.24	91.42	93.34	98.49

The sound field can roughly be broken down into three frequency ranges. The frequency range of interest is the range of frequencies where T-S waves are the most unstable and can cause transition. For the experimental configuration shown in Figure 2 and similar experiments, the frequency band where T-S waves contribute to transition is (roughly) 30 to 120 Hz. Sound with frequencies between 30 Hz and 120 Hz will be considered part of the 'T-S band' for the purpose of this thesis.

Low-frequency sound, caused by separation and unsteady flow pockets, does not have the same effect on transition as noise in the T-S band; however, the presence of these low-frequency oscillations can adversely affect experiments. Noise at higher frequencies does not strongly affect sound receptivity experiments; for example, the neutral stability curve shown in Figure 2 has a maximum unstable frequency near 350 Hz. Disturbances at frequencies above the T-S band are either stable or have small growth rates, so these disturbances affect transition less than disturbances in the T-S band.

Table 3 shows the total sound pressure level for each test point. The table also shows the contribution of the three frequency ranges to the sound pressure level. The majority of the pressure fluctuations in the tunnel are very low frequency. This trend is

especially true at higher speeds; at 1000 RPM, p_{rms} of the low frequency content is over 94% of the total p_{rms}.

Table 3. Breakdown of baseline SPL by frequency range

RPM	Freestream Speed (m/s)	Total SPL (dB)	Low Frequency Contribution (< 30 Hz) (dB)	T-S Band Contribution (30 Hz – 120 Hz) (dB)	Higher Frequency Contribution (120 Hz – 5 kHz) (dB)
200	5.27	75.16	74.55	65.13	60.38
400	11.21	86.81	86.44	73.66	72.05
600	17.24	93.68	93.21	79.02	81.98
800	23.29	100.09	99.62	84.20	88.96
1000	29.40	105.45	104.94	88.87	95.00

Saric and Reshotko (1998) recommend that the rms static pressure fluctuations be less than 0.3% of the freestream dynamic pressure. Table 4 shows the normalized rms pressure fluctuations measured by microphone one in the test section. The KSWT does not meet the 0.3% requirement for any of the test points. When compared to the dynamic pressure, the acoustic fluctuations are smallest in the middle of the speed range.

The low frequency content shown in Table 3 dominates the pressure fluctuation magnitudes shown in Table 4. For example, at 1000 RPM, the low frequency content needs to be decreased by 76% in order to meet the 0.3% criteria. These oscillations by themselves do not strongly affect transition; the growth rates associated with disturbances at these frequencies are small compared to growth rates in the T-S band.

These pressure fluctuations can be considered as an unsteady base flow rather than a disturbance that causes transition

Unsteady separation bubbles in contractions and/or diffusers may be the cause for the low frequency unsteadiness. Later in this section, cross correlations will be used to determine the source of the low noise.

Table 4. Baseline pressure fluctuations normalized by dynamic pressure

RPM	p_{rms} (Pa)	Freestream Speed (m/s)	q_∞ (Pa)	p_{rms}/q_∞ (%)
200	0.115	5.27	16.24	0.708
400	0.438	11.21	73.55	0.596
600	0.966	17.24	173.64	0.556
800	2.021	23.29	315.91	0.640
1000	3.746	29.40	500.74	0.748

Figure 8 shows the narrowband sound pressure level spectrum for the five test speeds. All of the speeds show the same spectrum trends; low frequency (< 30 Hz) noise is the largest contributor to the tunnel pressure fluctuations. Around 30 to 40 Hz, the spectrum drops approximately 10 dB, and tonal noise sources (motor and blade passing noise) become prevalent through the broadband noise. At higher frequencies, the spectra continue to drop to lower sound levels.

The colored lines at the top of Figure 8 represent frequencies where T-S waves can be unstable in a two-dimensional, zero pressure gradient boundary layer. The lowest frequency corresponds to a growth (or N) factor of nine, while the maximum frequency corresponds to the highest unstable frequency for that speed. The vertical black line

represents the planar cutoff frequency of the test section (120 Hz). 600 Hz (or 17.24 m/s with the swept wing experimental setup) is the fastest speed where unstable T-S waves with growth factors of nine or less correspond with planar waves in the test section.

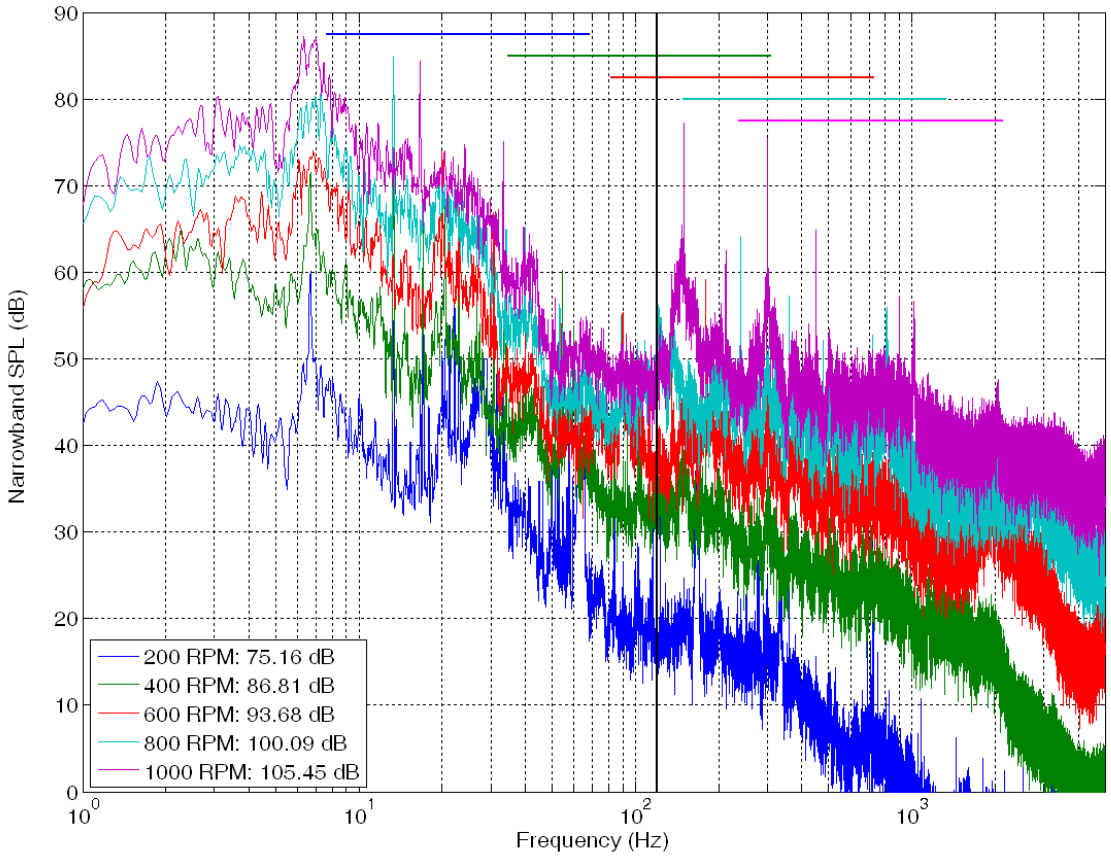

Figure 8. Test section narrowband SPL measured at microphone one across tunnel rpm range

3.2 Low-Frequency Oscillations

The origin of the low-frequency pressure fluctuations can't be determined through spectrum measurements. Cross correlations can isolate the directionality of

waves by examining the time lag between which two signals are the most correlated. The cross correlations were performed at 1000 RPM, the speed where the low frequency waves had the highest amplitude.

Five microphones were placed in different locations around the KSWT circuit; these locations are shown in Figure 9. The distance between each microphone (measured along the tunnel centerline) was divided by the speed of sound in the test section to calculate the estimated wave propagation lag between microphone locations. The lag is the time that it takes an acoustic wave to travel from one microphone location to another microphone location. The estimated time lag for one loop around the entire wind tunnel is approximately 155 ms.

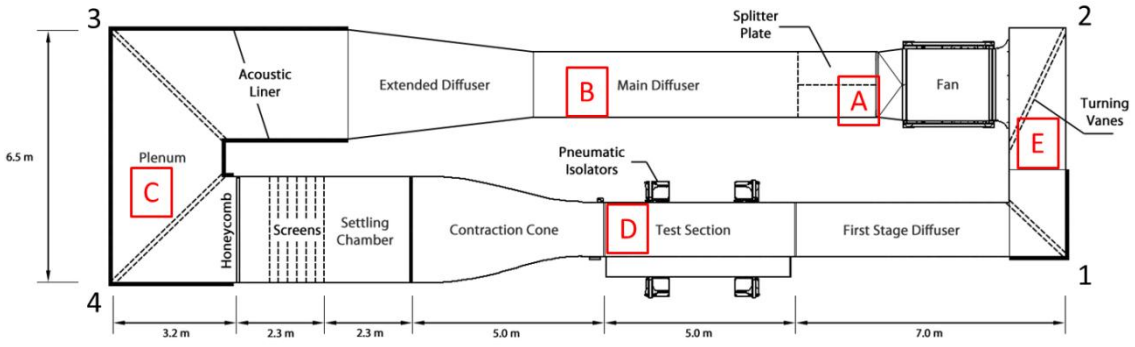

Figure 9. Microphone locations for low frequency correlation measurements

The actual propagation time lag between each microphone may vary from the predicted value. Wave direction, local air velocity, thermal gradients and the acoustic mode shape can all affect the rate at which sound travels through the tunnel. The estimated wave propagation lags are used to look for expected peaks in the correlations.

The correlations between the five microphones show that the predominant source of the low frequency unsteadiness is near microphone E. The correlation between microphone A and microphone B, shown in Figure 10, has a maximum value associated with unsteadiness traveling downstream through the main diffuser. The correlation between microphone A and microphone E, shown in Figure 11, also has a maximum value for waves traveling downstream from microphone E to microphone A. The correlation between microphone E and microphone D, shown in Figure 12, has a maximum value for waves traveling upstream into the test section. The three correlations show that a source of low frequency unsteadiness near microphone E is propagating both upstream and downstream into other areas of the tunnel.

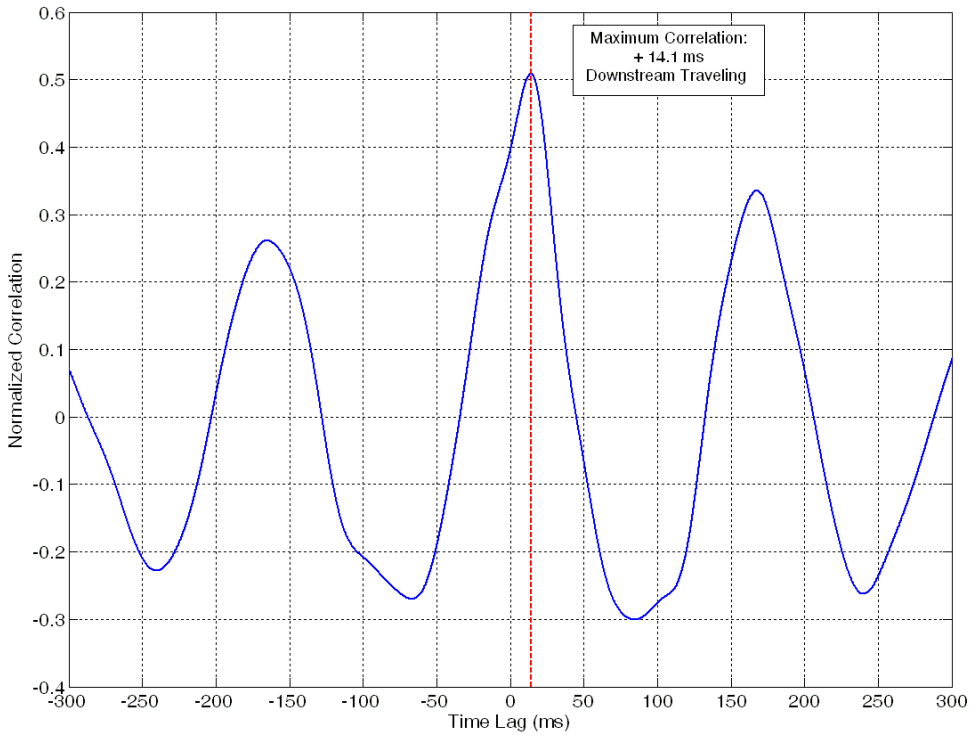

Figure 10. Correlation between microphone A (reference) and microphone B

Microphone E is located between corner one and corner two. In this section of the tunnel, the flow travels through a contraction before passing through a rectangular to circular transition that leads into the fan housing. Either of these features could be causing a separation bubble that would explain the unsteadiness. Because the fan is also located near microphone E, unsteadiness in fan RPM was also considered as a source; however, a proximity sensor on the fan shaft showed that the fan RPM remains constant when the motor RPM is set to a particular value.

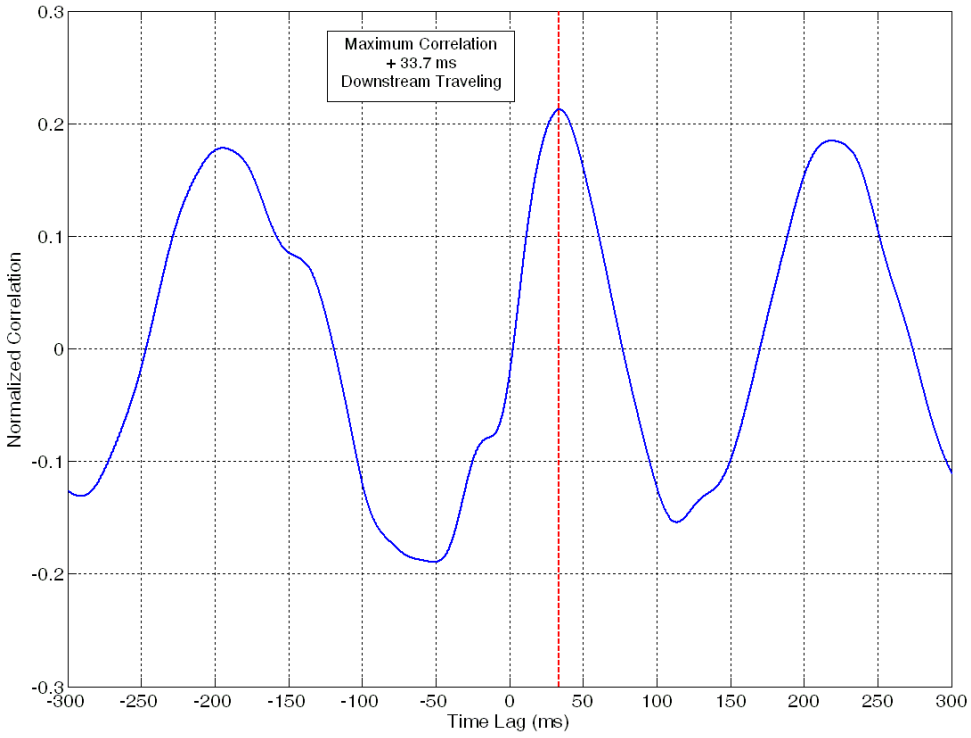

Figure 11. Correlation between microphone E (reference) and microphone A

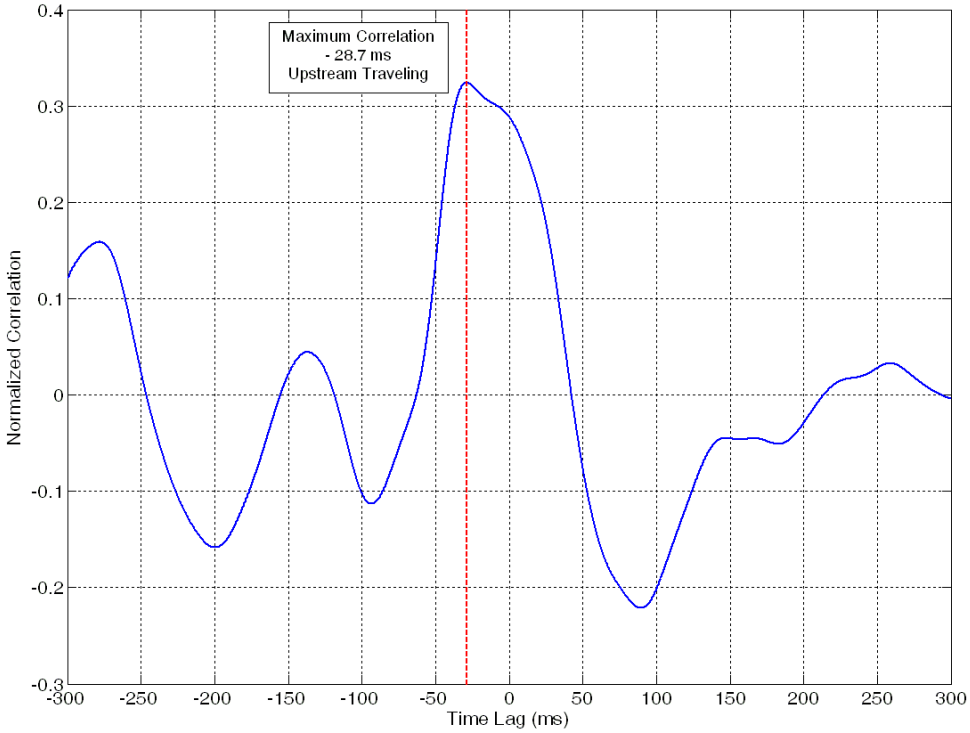

Figure 12. Correlation between microphone D (reference) and microphone E

The correlations also show a secondary source of unsteadiness in the tunnel located in the extended diffuser. Figure 13 shows the correlation between microphone C and microphone A. Based on the distance between the two microphones, the expected maximum correlation should occur near ± 57 ms. Instead, the maximum correlation occurs near -26 ms. The correlation between microphone C and microphone B, shown in Figure 14, also has a two-peak structure. The second peak is caused by a source of fluctuations between the two microphones; the fluctuations travel upstream and downstream and explain the correlation of the two signals at a time lag less than the acoustic time lag.

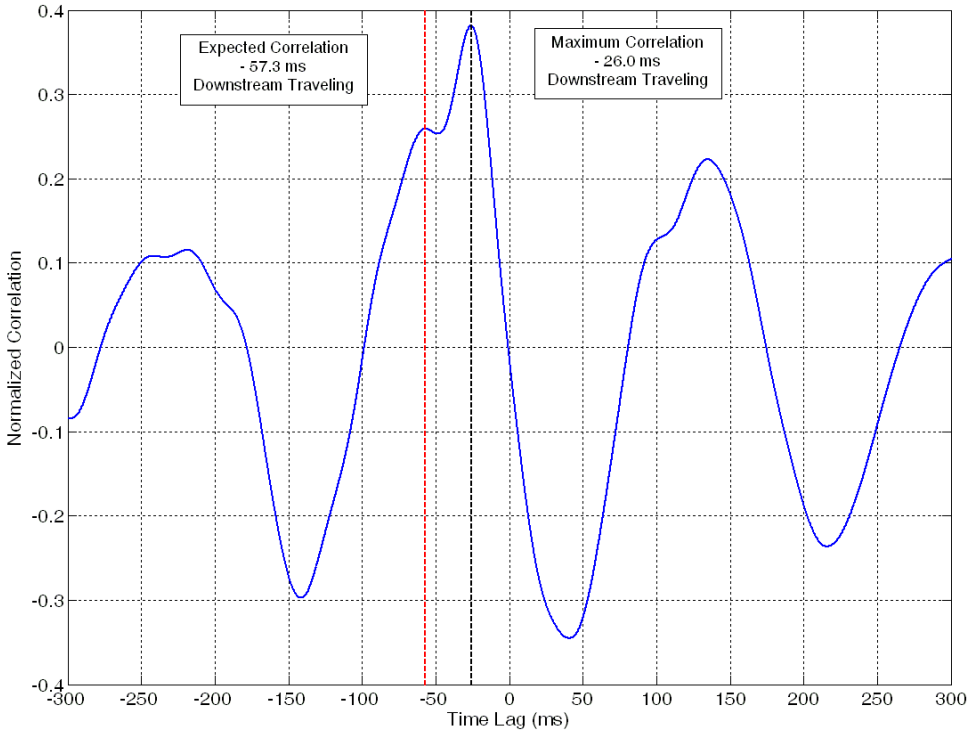

Figure 13. Correlation between microphone C (reference) and microphone A

The correlation between microphone D and microphone A, shown in Figure 15, also has a double-peak structure similar to Figure 13 and Figure 14. The maximum correlation occurs at -97.4 ms, which is related to waves traveling downstream through the plenum and into the test section. A smaller correlation occurs at + 63.1 ms, which is related to waves traveling upstream into the test section. Another correlation appears at +87.4 ms; the spacing of the two peaks is similar to the peaks seen in Figure 13 and Figure 14, and the +87.4 ms peak does not correspond to waves traveling upstream between the microphones. The second peak is most likely caused by the same source that causes a similar pattern in the other two correlations.

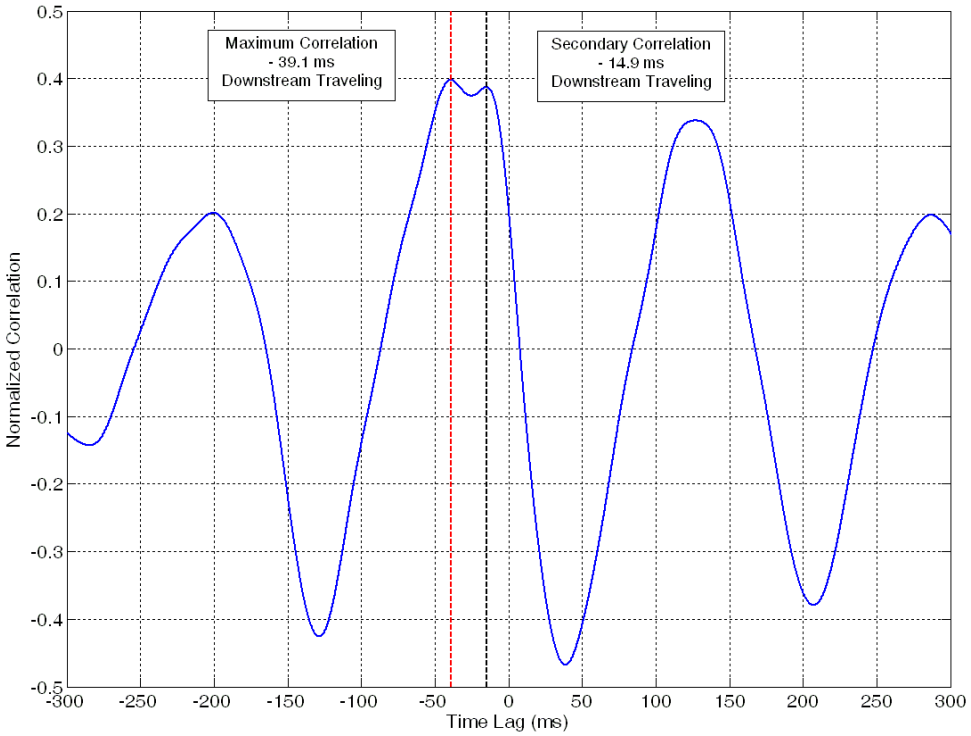

Figure 14. Correlation between microphone C (reference) and microphone B

The most likely cause of unsteadiness in a diffuser is a region of recirculating, unattached flow. As the flow travels through the extended diffuser, the adverse pressure gradient can cause the boundary layer to detach. During construction, a vertical splitter plate was installed to reduce the diffuser angle and prevent flow detachment. The splitter plate is supported by struts that attach to the walls at mid-span to prevent vibration; however, vibration and structural effects of the splitter plate may also be contributing to the problem.

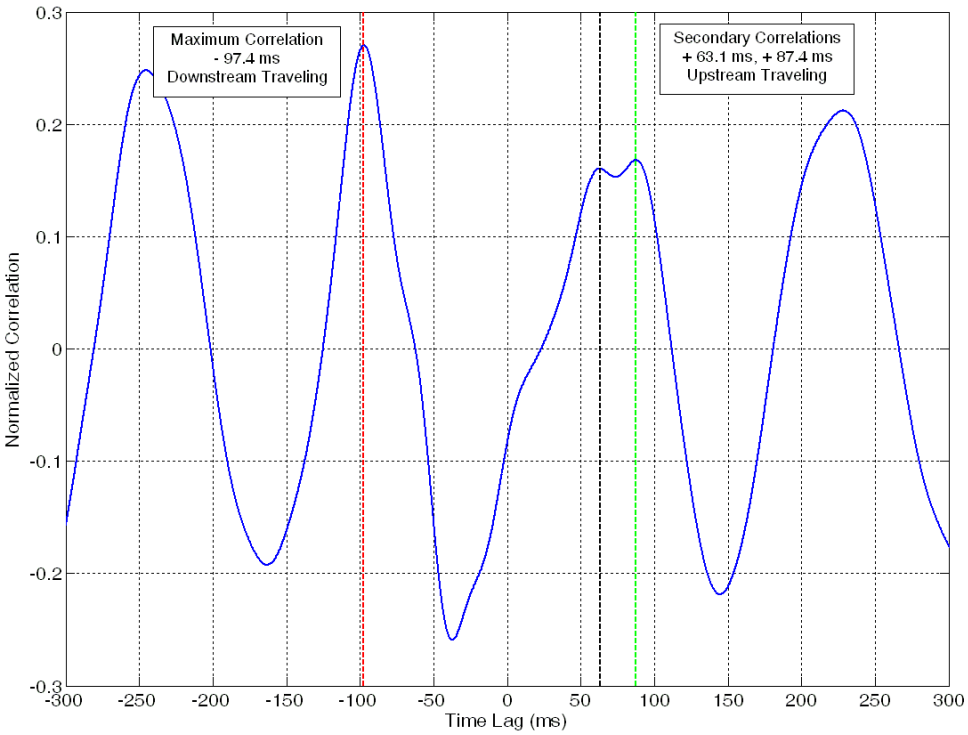

Figure 15. Correlation between microphone D (reference) and microphone A

3.3 Motor Frequencies

The noise spectrum in the test section has both tonal and broadband components. The tonal components of the signal can be attributed to motor and blade passing noise. Although the motor is outside of the tunnel, motor noise can propagate through the fan enclosure into the flow. For the KSWT, the motor frequency is not in the range of T-S waves; however, motor noise can contribute to the low frequency fluctuations that are prevalent in the tunnel. Table 5 shows the motor frequencies and sound pressure levels for the six test speeds. In general, the amount of motor noise increases as tunnel speed is increased.

Table 5. Motor frequency noise - baseline case

RPM	Motor Frequency (Hz)	Motor Frequency SPL (dB)	1st Harmonic SPL (dB)	2nd Harmonic SPL (dB)
200	3.33	53.57	65.35	52.51
400	6.67	77.58	76.62	74.84
600	10.00	73.83	79.05	64.17
800	13.33	89.19	73.96	70.12
1000	16.67	89.36	79.62	61.63

The two microphone, single-direction sensing technique was used to decompose the microphone signals into upstream and downstream traveling components. The narrowband SPL was then calculated for both components, and the motor sound pressure levels were extracted from the spectrum. Table 6 shows the directional decomposition of the motor noise, while Table 7 shows the relative magnitude of the upstream traveling component compared to the downstream traveling component. Frequencies below 10 Hz were not analyzed due to the error in the single direction sensing technique at those low frequencies. Both tables show that motor noise primarily travels upstream into the test section.

Table 6. Directional decomposition of motor noise

RPM	Motor Frequency		1st Harmonic		2nd Harmonic	
	Upstream (dB)	Downstream (dB)	Upstream (dB)	Downstream (dB)	Upstream (dB)	Downstream (dB)
200	-	-	-	-	51.67	50.44
400	-	-	72.02	74.53	75.56	64.36
600	70.12	70.91	77.37	75.10	65.04	58.59
800	85.68	85.41	73.12	66.24	68.45	62.28
1000	88.19	84.23	82.84	73.59	63.99	62.12

Table 7. Relative magnitude of upstream and downstream traveling motor noise

RPM	Motor Frequency (dB)	1st Harmonic (dB)	2nd Harmonic (dB)
200	-	-	1.23
400	-	-2.51	11.20
600	-0.78	2.27	6.46
800	0.27	6.89	6.16
1000	3.97	9.26	1.87

3.4 Blade Passing Frequencies

Blade passing noise is another source of tonal noise in the tunnel. The KSWT is driven by a nine-bladed fan, so the blade passing frequency is nine times the motor frequency. Blade passing noise can be in the unstable T-S band, so test frequencies should be placed as far away as possible from the blade passing frequency.

Table 8 shows the sound pressure level at the blade passing frequency for the six test points. The blade passing noise increases with tunnel speed and has harmonics that, in most cases, decrease in amplitude. The blade passing frequency and first two harmonics are narrowband peaks in the spectra that rise at least 10 dB around the surrounding noise. The third harmonic and higher harmonics are not distinguishable from tunnel background noise.

Table 8. Blade passing noise - baseline case

RPM	Blade Passing Frequency (Hz)	Blade Passing Frequency SPL (dB)	1st Harmonic SPL (dB)	2nd Harmonic SPL (dB)
200	30.00	51.36	43.65	32.71
400	60.00	58.81	49.82	49.51
600	90.00	61.45	64.00	53.96
800	120.00	74.51	68.61	62.30
1000	150.00	81.94	79.83	69.56

Table 9 shows the directional decomposition of blade passing noise, while Table 10 shows the relative magnitude of upstream traveling blade passing noise to downstream traveling blade passing noise. Frequencies above the planar cutoff frequency of the test section were also not analyzed because the sensing technique assumes planar waves.

Table 9. Directional decomposition of blade passing noise

RPM	Blade Passing Frequency		1st Harmonic		2nd Harmonic	
	Upstream (dB)	Downstream (dB)	Upstream (dB)	Downstream (dB)	Upstream (dB)	Downstream (dB)
200	53.81	53.89	46.89	38.12	33.54	26.43
400	59.18	53.57	49.89	45.70	-	-
600	59.65	51.91	-	-	-	-
800	70.40	68.11	-	-	-	-
1000	-	-	-	-	-	-

Both tables show that blade passing noise primarily travels upstream from the fan into the test section. The section of the tunnel in-between the fan and the test section has

only a small amount of acoustic treatments, while tonal noise traveling downstream goes through the plenum which is lined with acoustic treatments. The acoustic treatments may explain why motor and blade passing noise primarily travels upstream into the test section.

Table 10. Relative magnitude of upstream and downstream traveling fan noise

RPM	Blade Passing Frequency	1^{st} Harmonic	2^{nd} Harmonic
200	-0.09	8.77	7.11
400	5.61	4.19	-
600	7.74	-	-
800	2.28	-	-
1000	-	-	-

4. THE EFFECT OF TUNNEL ACOUSTIC TREATMENTS

During the construction of the KSWT at Texas A&M, acoustic foam and broadband acoustic paneling were installed in several locations in the tunnel. The effectiveness of the treatments was never measured; the acoustic treatments were installed before any microphone measurements were made. The foam and panels were covered using plywood, and microphone measurements with the plywood coverings installed show how much sound is removed from the flow by the acoustic treatments.

4.1 Installation of Acoustic Treatment Coverings

The acoustic treatments were covered using 5 mm thick plywood. Thin plywood was chosen due to ceiling weight constraints and installation considerations. The plywood was attached to ceilings, walls and floors over the foam and acoustic panels in the tunnel. Large sheets of plywood were connected to the walls and ceiling using ¼" threaded rods, while smaller panels were supported by adhesive backed hook and loop fasteners. Each panel was stapled to the surrounding panels, and the seams between plywood sheets were taped to prevent the plywood from flapping during measurements.

The plywood was installed in four stages. During each stage, a different section of the tunnel was covered with plywood. The foam and panels on the walls in corner one were covered during the first stage. During stage two, plywood was placed over the foam and panels between the extended diffuser and the corner three turning vanes. The acoustic treatments between corner three and corner four turning vanes were covered during stage three, while the acoustic treatments between the corner four turning vanes were installed during stage four. A diagram showing the progression of the acoustic

treatment coverings can be seen in Figure 16. Figure 17 and Figure 18 show pictures of the installed plywood treatments in zones two and three.

In order to remove the effect of the acoustic treatments, the plywood needs to reflect all incident sound waves. When used as a baffle, 5 mm plywood allows the majority of sound to pass through it due to a small panel thickness and stiffness. In this situation, the plywood is mounted against stiff acoustic foam and metal acoustic panels. The stiffness of the foam and panels will prevent the plywood from flexing and moving, and in the process, will create an acoustically rigid surface.

In the following subsections, gray entries in tables indicate an increase in the noise level as compared to the baseline case. The addition of the plywood coverings should increase noise levels in the tunnel, so gray table entries indicate an expected increase in the sound level.

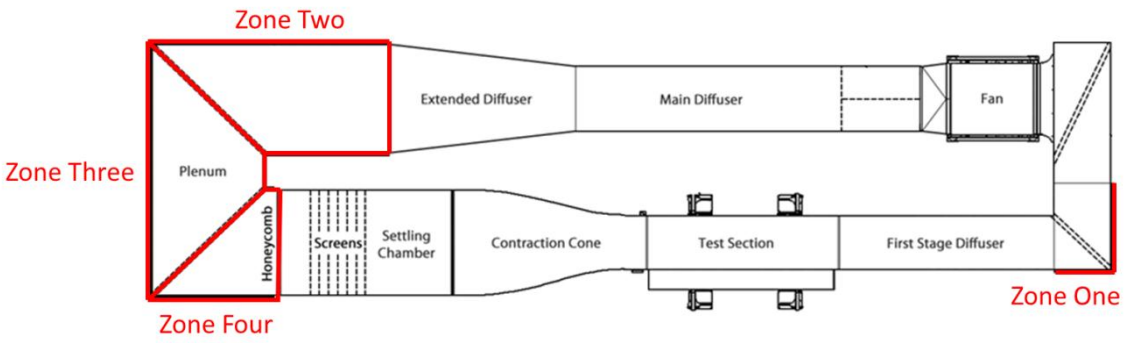

Figure 16. Progression of plywood coverings for acoustic treatments

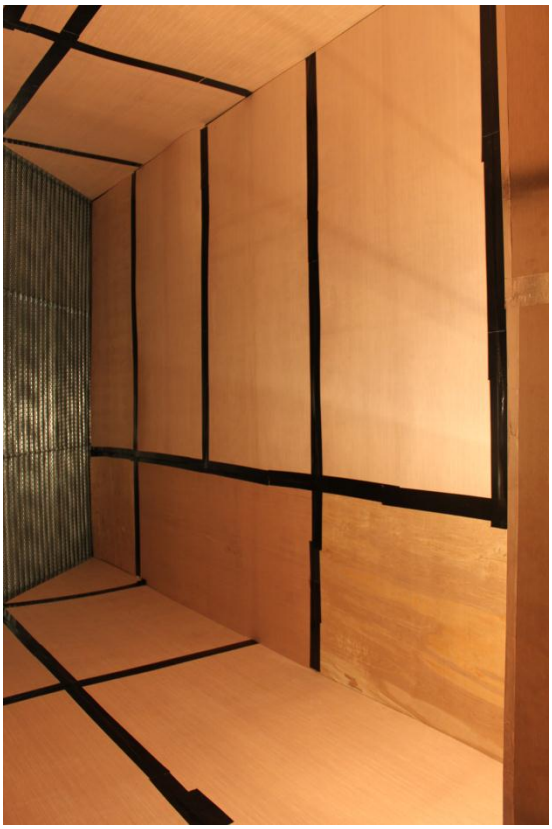

Figure 17. Plywood coverings in zone two

Figure 18. Plywood coverings in zone three

4.2 Effect of Acoustic Treatments in Corner One

The 81 ft^2 of foam lining the outside walls of corner one was the first tunnel section covered in plywood. The small cross sectional area in corner one limits the space for acoustic treatments. After the plywood was installed, microphone measurements documented the sound pressure level and the pressure spectrum.

The acoustic treatments in corner one did not have a large impact on test section noise levels. Table 11 shows the sound pressure level relative to the baseline case. The coverings increased the high frequency content for all five speeds and raised the overall SPL at four of the five speeds, but all of the changes are moderate.

Table 11. Sound pressure level with acoustic treatments in corner one covered

RPM	Freestream Speed (m/s)	Total SPL (dB)	Low Frequency Contribution (< 30 Hz) (dB)	T-S Band Contribution (30 Hz – 120 Hz) (dB)	Higher Frequency contribution (120 Hz – 5 kHz) (dB)
200	5.27	75.88 (+ 0.72 dB)	75.41 (+0.86 dB)	64.33 (-0.80 dB)	60.96 (+ 0.58 dB)
400	11.21	87.94 (+1.13 dB)	87.62 (+1.18 dB)	73.56 (-0.10 dB)	73.46 (+ 1.41 dB)
600	17.24	93.67 (- 0.01 dB)	93.02 (- 0.19 dB)	79.68 (+ 0.66 dB)	83.56 (+ 1.58 dB)
800	23.29	100.19 (+ 0.10 dB)	99.58 (- 0.04 dB)	85.05 (+ 0.85 dB)	90.24 (+ 1.28 dB)
1000	29.40	105.79 (+ 0.34 dB)	105.14 (- 0.20 dB)	89.74 (+ 0.87 dB)	96.40 (+ 1.40 dB)

Table 12 shows the effect of the corner one acoustic treatments on motor noise levels while Table 13 shows the sound pressure level of blade passing noise. The change

in the sound levels is not consistent with speed; at lower speeds, the acoustic treatments significantly affected motor noise while not affecting blade passing noise. In contrast, at higher speeds, the acoustic treatments have a significant effect on blade passing noise while not affecting motor noise. The effect of the treatments at a constant frequency are also not consistent with speed; the 600 RPM motor frequency, 400 RPM first harmonic and 200 RPM second harmonic all occur at 10 Hz, but the effect of the treatments varies between the three cases.

Table 12. Motor frequency noise with acoustic treatments in corner one covered

RPM	Motor Frequency (Hz)	Motor Frequency SPL (dB)	1st Harmonic SPL (dB)	2nd Harmonic SPL (dB)
200	3.33	53.66 (+ 0.09)	68.51 (+ 3.16)	51.54 (- 0.97)
400	6.67	82.30 (+ 4.72)	77.25 (+ 0.63)	74.79 (- 0.05)
600	10.00	73.18 (- 0.65)	79.00 (- 0.05)	62.39 (- 1.78)
800	13.33	88.13 (- 1.06)	75.20 (+ 1.24)	70.31 (+ 0.19)
1000	16.67	89.60 (+ 0.24)	79.67 (+ 0.05)	61.24 (- 0.39)

Table 13. Blade passing noise with acoustic treatments in corner one covered

RPM	Blade Passing Frequency (Hz)	Blade Passing Frequency SPL (dB)	1st Harmonic SPL (dB)	2nd Harmonic SPL (dB)
200	30.00	53.37 (+ 2.01)	37.94 (- 5.71)	31.55 (- 1.16)
400	60.00	58.58 (- 0.23)	49.26 (- 0.56)	52.65 (+ 3.14)
600	90.00	64.49 (+ 3.04)	66.32 (+ 2.32)	55.75 (+ 1.79)
800	120.00	73.64 (- 0.87)	73.81 (+ 5.20)	61.23 (- 1.07)
1000	150.00	84.89 (+ 2.95)	81.52 (+ 1.69)	70.87 (+ 1.31)

Table 14 shows the directional decomposition of motor noise in the test section with the corner one treatments covered, while Table 15 shows the directional decomposition of blade passing noise with the corner one treatments covered. The directional results do not show a consistent pattern. The expected effect of the corner one acoustic treatments was to remove upstream traveling noise; covering the treatments did not create a consistent increase or decrease in the directional components of tonal noise in the test section. The upstream traveling motor and blade passing noise remains louder than the downstream traveling component with the corner one acoustic treatments covered.

Table 14. Directional decomposition of motor noise with acoustic treatments in corner one covered

	Motor Frequency		1st Harmonic		2nd Harmonic	
RPM	Upstream (dB)	Downstream (dB)	Upstream (dB)	Downstream (dB)	Upstream (dB)	Downstream (dB)
200	-	-	-	-	51.73 (+ 0.06)	51.78 (+ 1.34)
400	-	-	72.91 (+ 0.89)	75.07 (+ 0.54)	75.39 (- 0.17)	64.13 (- 0.23)
600	74.47 (+ 4.35)	73.82 (+ 2.91)	77.12 (- 0.25)	75.43 (+ 0.33)	63.42 (- 1.62)	59.86 (+ 1.27)
800	84.40 (- 1.28)	83.68 (- 1.73)	73.25 (+ 0.13)	67.17 (+ 0.93)	68.49 (+ 0.04)	61.83 (- 0.45)
1000	88.76 (+ 0.57)	84.18 (- 0.05)	82.96 (+ 0.12)	73.71 (+ 0.12)	62.64 (- 1.35)	63.25 (+ 1.13)

Table 15. Directional decomposition of blade passing noise with acoustic treatments in corner one covered

	Blade Passing Frequency		1st Harmonic		2nd Harmonic	
RPM	Upstream (dB)	Downstream (dB)	Upstream (dB)	Downstream (dB)	Upstream (dB)	Downstream (dB)
200	51.25 (- 2.56)	50.35 (- 3.54)	41.38 (- 5.51)	40.44 (+ 2.32)	32.06 (- 1.48)	28.09 (+ 1.66)
400	58.74 (- 0.44)	52.22 (- 1.35)	50.60 (+ 0.71)	47.56 (+ 1.86)	-	-
600	63.47 (+ 3.82)	51.36 (- 0.55)	-	-	-	-
800	69.12 (- 1.28)	66.86 (- 1.25)	-	-	-	-
1000	-	-	-	-	-	-

Figure 19 compares the narrowband SPL in the test section with and without the corner one acoustic treatments at 600 RPM. The effect of the acoustic treatments is clearly seen at high frequencies; the baseline case has lower broadband noise levels at

higher frequencies. The effect of acoustic treatments on the low frequency content and tonal noise in the T-S band is negligible.

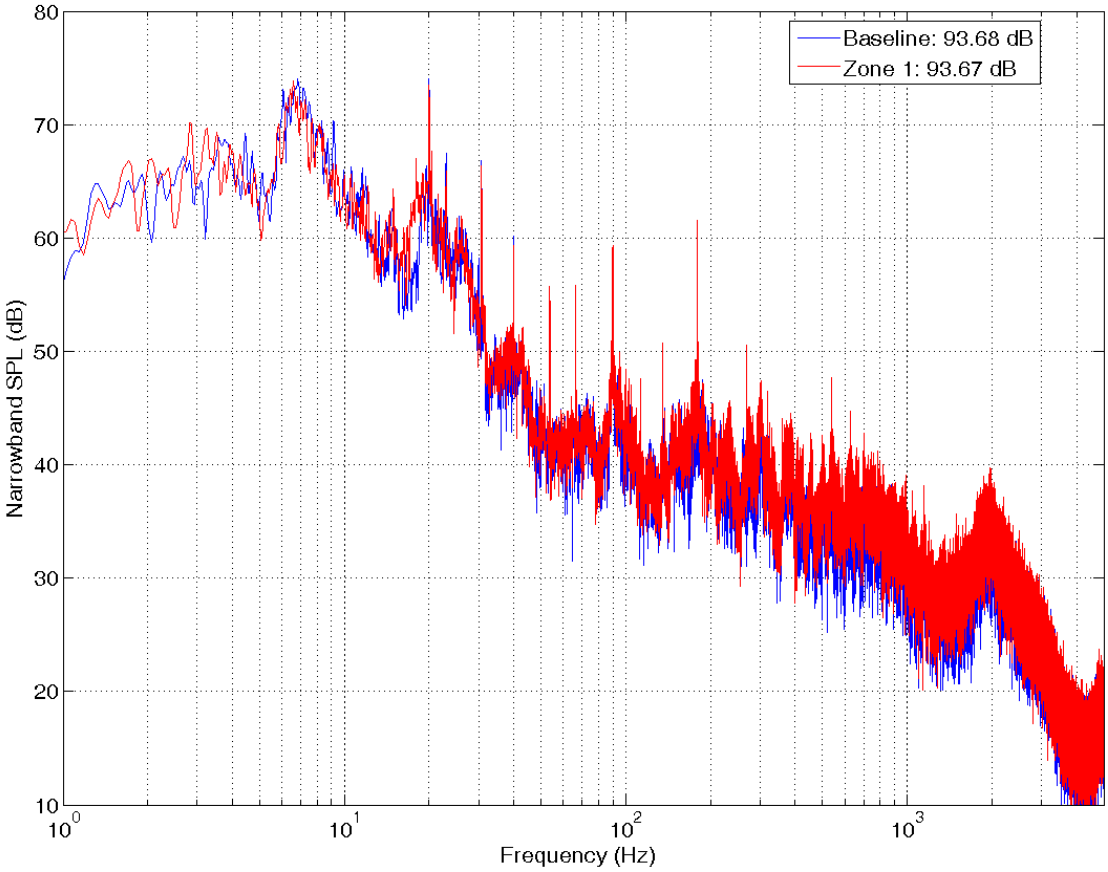

Figure 19. Comparison of pressure spectra for baseline case and zone 1 covered at 600 RPM

The plywood coverings in corner one were removed before all four zones of coverings were finished. Corner one is a high speed area in the tunnel; the cross sectional area is only 1.74 times greater in corner one than in the test section. During testing, the trailing edge of panels in corner one began to flutter. The flapping created an

unsteady loading on the fan which caused the motor controller to rapidly adjust rpm to compensate. The panels were removed in order to prevent damage to the motor, belt and pulley system.

4.3 Effect of Acoustic Treatments in Plenum

After the coverings were removed from corner one, plywood was installed to cover all of the acoustic treatments in the plenum. The surface area of the tunnel is largest in the plenum; over 1267 ft^2 of acoustic treatment line the walls, floors, and ceilings in this section of the tunnel.

As expected, the acoustic treatments in the plenum have a noticeable effect on the noise level inside the tunnel. Table 16 shows the sound pressure level in the test section with plywood covering the plenum acoustic treatments. The noise levels increased across all frequency bands; in particular, the high frequency band noise increased over 2 dB at four of the five speeds. The increase in overall SPL is small and varies from +0.33 dB to +0.91 dB. Unfortunately, the acoustic treatments have the largest impact on the higher frequency band rather than the low frequency band and the T-S band.

Table 16. Sound pressure level with acoustic treatments in plenum covered

RPM	Freestream Speed (m/s)	Total SPL (dB)	Low Frequency Contribution (< 30 Hz) (dB)	T-S Band Contribution (30 Hz – 120 Hz) (dB)	Higher Frequency Contribution (120 Hz – 5 kHz) (dB)
200	5.27	75.66 (+ 0.50 dB)	75.24 (+ 0.69 dB)	63.48 (+ 2.35 dB)	60.62 (+ 0.24 dB)
400	11.21	87.70 (+ 0.89 dB)	87.27 (+ 0.83 dB)	74.38 (+ 0.72 dB)	74.40 (+ 2.35 dB)
600	17.24	94.01 (+ 0.33 dB)	93.35 (+ 0.14 dB)	79.29 (+ 0.27 dB)	84.24 (+ 2.26 dB)
800	23.29	101.00 (+ 0.91 dB)	100.40 (+ 0.78 dB)	84.50 (+ 0.30 dB)	91.30 (+ 2.34 dB)
1000	29.40	106.15 (+ 0.70 dB)	105.47 (+ 0.53 dB)	89.40 (+ 0.53 dB)	97.09 (+ 2.09 dB)

The acoustic treatments are also effective at removing motor and blade passing noise from the tunnel. Table 17 shows the effect of the plenum acoustic treatments on motor noise and harmonics of motor noise, while Table 18 shows the effect of the acoustic treatments on blade passing noise. For all of the test points, the motor noise in the test section increased at least 2 dB. With the exception of one test point, the level of the motor harmonics also all increased. The plywood coverings also created a large increase in blade passing noise. With the exception of 200 RPM, the harmonics of the blade passing frequency increased in amplitude. The plenum acoustic treatments do an excellent job at removing tonal noise, even at low frequencies.

Table 17. Motor noise with acoustic treatments in plenum covered

RPM	Motor Frequency (Hz)	Motor Frequency SPL (dB)	1st Harmonic SPL (dB)	2nd Harmonic SPL (dB)
200	3.33	55.11 (+ 1.54)	68.60 (+ 3.25)	51.88 (- 0.63)
400	6.67	82.37 (+ 4.79)	75.29 (- 1.33)	76.28 (+ 1.44)
600	10.00	78.79 (+ 4.96)	79.17 (+ 0.12)	65.43 (+ 1.26)
800	13.33	90.00 (+ 0.81)	76.66 (+ 2.70)	71.48 (+ 1.36)
1000	16.67	90.32 (+ 0.96)	79.99 (+ 0.37)	66.08 (+ 4.45)

Table 18. Blade passing noise with acoustic treatments in plenum covered

RPM	Blade Passing Frequency (Hz)	Blade Passing Frequency SPL (dB)	1st Harmonic SPL (dB)	2nd Harmonic SPL (dB)
200	30.00	55.86 (+ 4.50)	33.97 (- 9.68)	29.91 (- 2.80)
400	60.00	59.52 (+ 0.71)	50.34 (+ 0.52)	50.51 (+ 1.00)
600	90.00	63.55 (+ 2.10)	65.65 (+ 1.65)	59.01 (+ 5.05)
800	120.00	75.07 (+ 0.56)	72.68 (+ 4.07)	63.75 (+ 1.45)
1000	150.00	84.40 (+ 2.46)	80.66 (+ 0.83)	72.26 (+ 2.70)

Table 19 and Table 20 show the directional decomposition of motor noise and blade passing noise, respectively, with the acoustic treatments in the plenum covered. The expected result was an increase in the downstream traveling waves while not strongly affecting the upstream traveling waves. This pattern is not present in the

directional decomposition data; for example, the upstream traveling noise at the motor frequency increased for 600, 800, and 1000 RPM, but the downstream traveling noise was not as strongly affected. Either the acoustic treatments have a more complicated effect on the directionality of waves than expected, or the single-direction sensing technique is not able to reliably extract the upstream and downstream traveling components from the broadband microphone signals.

Table 19. Directional decomposition of motor noise with acoustic treatments in plenum covered

	Motor Frequency		1st Harmonic		2nd Harmonic	
RPM	Upstream (dB)	Downstream (dB)	Upstream (dB)	Downstream (dB)	Upstream (dB)	Downstream (dB)
200	-	-	-	-	53.64 (+ 1.97)	50.58 (+ 0.14)
400	-	-	72.85 (+ 0.83)	71.53 (- 3.00)	75.11 (- 0.45)	62.94 (- 1.42)
600	72.16 (+ 2.04)	68.16 (- 2.75)	76.22 (- 1.15)	75.55 (+ 0.45)	66.73 (+ 1.69)	63.72 (+ 5.13)
800	87.64 (+ 1.96)	85.38 (- 0.03)	72.63 (- 0.49)	70.91 (+ 4.67)	68.33 (- 0.12)	65.30 (+ 3.02)
1000	89.37 (+ 1.18)	84.94 (+ 0.71)	81.58 (- 1.26)	71.93 (- 1.66)	66.93 (+ 2.94)	63.69 (+ 1.57)

Table 20. Directional decomposition of blade passing noise with acoustic treatments in plenum covered

	Blade Passing Frequency		1st Harmonic		2nd Harmonic	
RPM	Upstream (dB)	Downstream (dB)	Upstream (dB)	Downstream (dB)	Upstream (dB)	Downstream (dB)
200	53.64 (- 0.17)	55.11 (+ 1.22)	39.85 (- 7.04)	39.52 (+ 1.40)	31.89 (- 1.65)	26.02 (- 0.41)
400	59.98 (+ 0.80)	50.64 (- 2.93)	49.80 (- 0.09)	46.74 (+ 1.04)	-	-
600	62.20 (+ 2.55)	51.15 (- 0.76)	-	-	-	-
800	70.10 (- 0.30)	69.83 (+ 1.72)	-	-	-	-
1000	-	-	-	-	-	-

Figure 20 compares microphone spectra with and without the coverings in the plenum at 600 RPM. The comparison clearly shows increased broadband noise both in the T-S wave band and at higher frequencies. The spectrum also shows that the tonal noise is louder with the acoustic treatments covered.

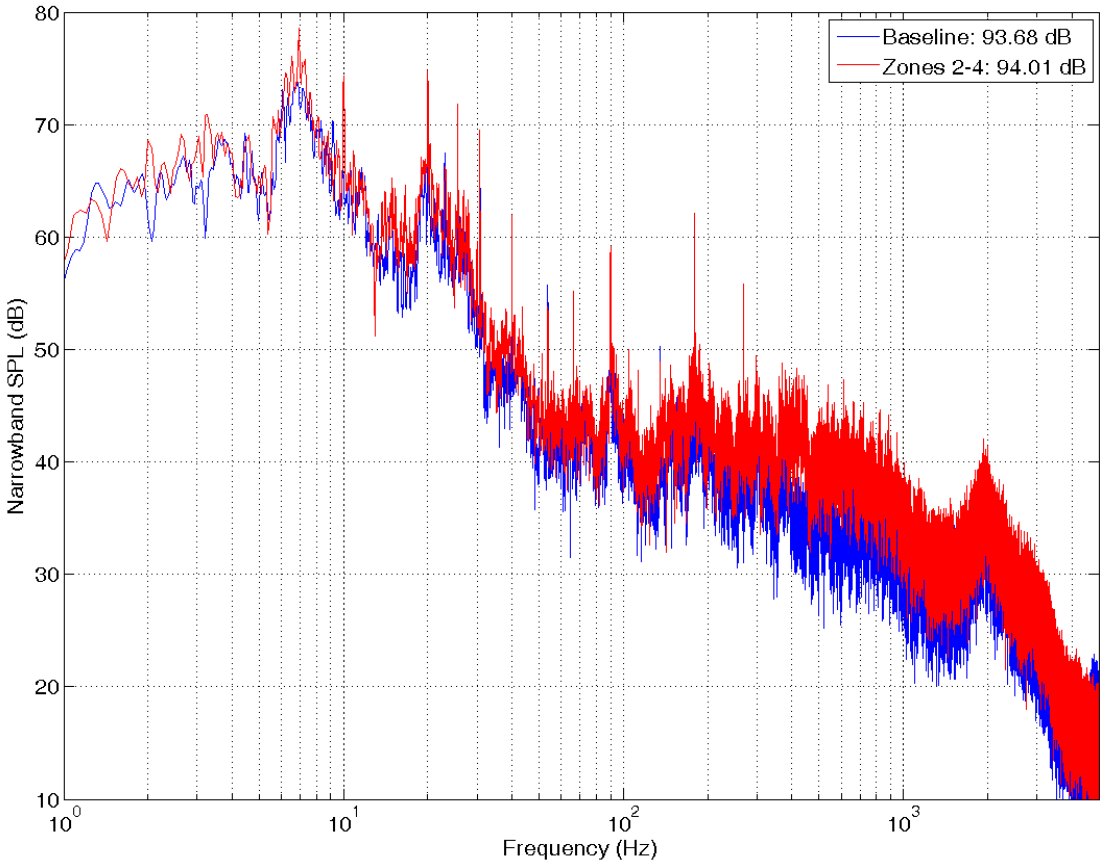

Figure 20. Comparison of pressure spectra for baseline case and zones 2-4 covered at 600 RPM

A crosswire was used to measure the effect of the plenum acoustic treatments on turbulence levels. Results are compared to Hunt and Saric (2011), who made equivalent crosswire measurements with the baseline configuration. The crosswire measurements were AC coupled with a 1 Hz – 10 kHz band-pass.

Table 21 shows the effect of the acoustic treatments on disturbance intensities. The streamwise component (u') contains contributions from both sound and turbulence, while the transverse component (v') is more indicative of turbulence levels. The

transverse disturbance intensities did not increase more than the repeatability of the measurements (± 0.005 %); thus, the acoustic treatments have a limited effect on the turbulence levels in the tunnel. The effect of the acoustic treatments was larger on the streamwise fluctuations. At 600 RPM and 1000 RPM, the streamwise fluctuations increased more than the repeatability limit. This indicates that the acoustic treatments remove streamwise fluctuations from the flow.

Table 21. Effect of plenum acoustic treatments on crosswire disturbance intensities

Freestream Speed (m/s)	u'/U_o (%)		v'/U_o (%)	
	Baseline	Zones 2-4	Baseline	Zones 2-4
5	0.020	0.020	0.015	0.017
10	0.046	0.048	0.032	0.035
15	0.050	0.059	0.012	0.014
20	0.069	0.072	0.016	0.017
25	0.093	0.099	0.018	0.021

The increase in the streamwise velocity fluctuations matches the increase in the pressure fluctuations with the plenum acoustic treatments covered. The induced velocity of a planar acoustic wave is proportional to the associated pressure fluctuation, so the percentage increase in each quantity should also be proportional. The average increase in the root mean square pressure over five tunnel RPM settings (200, 400, 600, 800, and 1000 RPM) was 8.0%, while the average increase in the streamwise velocity fluctuation at five tunnel speeds (5, 10, 15, 20, and 25 m/s) was 6.6%. The two increases match each other within the repeatability of the turbulence measurements.

The acoustic treatments in the plenum remove both tonal noise in the T-S band and broadband, high frequency noise from the tunnel. The acoustic treatments in the plenum also slightly reduce the magnitude of the low frequency pressure oscillations. Further improvements to the KSWT should focus on removing the two sources of low frequency pressure oscillations and adding more acoustic treatments upstream of the test section.

5. CONTINUOUS ACOUSTIC FORCING: INFRASTRUCTURE UPGRADES AND TEST SECTION SOUND FIELD

Section 1 outlined the need to input acoustic disturbances at a known frequency into a wind tunnel experiment. Introducing known disturbances into the flow and measuring the receptivity provides insight into how different mechanisms affect transition.

A wall of speakers was installed at the KSWT in order to introduce downstream traveling acoustic disturbances into the flow. The sound created during acoustic forcing was measured in the test section. Single-direction sensing was also used to measure reflected waves created by the acoustic forcing.

5.1 Sound Generation Hardware

The sound waves used for acoustic receptivity measurements are generated by McCauley 6222 subwoofers. These 10” diameter subwoofers have a flat frequency response (± 3 dB) between 30 Hz and 2.5 kHz. The low frequency response of these subwoofers makes them ideal for low-speed receptivity studies; unstable T-S waves for typical experimental setups range from 40 Hz to 120 Hz.

The speakers are forced using a HP 33120A analog function generator. The output of the function generator is split into three channels, and each channel is amplified by a factor of 23 through an ADCOM GFA 555-II amplifier. The output from the three amplifiers is used to drive the five subwoofers. In order to not overload the 300

W continuous power capacity of the speakers, the input to the amplifiers should be held under 1.50 V_{rms}.

5.2 Speaker Wall Placement and Installation

The speakers were installed on the West wall of corner four. In this location, the speakers emit downstream traveling sound towards the test section without creating blockage inside the tunnel. The speakers were installed in a cross pattern along the wall and are centered with the test leg of the tunnel so the majority of acoustic energy travels downstream towards the test section. When the speakers are not needed, foam inserts can be placed over the speakers inside the tunnel to create a flat interior surface. The layout of the speaker wall inside of the tunnel is shown in Figure 21.

The basket of each speaker is inside of a plywood box located outside of the tunnel. Each box is approximately 7.6 ft^3 in volume; the volume of each box was maximized without blocking a walkway behind the West exterior wall of the wind tunnel. The interior of the box is vented to the plenum to equalize the pressure on the speaker face. Figure 22 shows pictures of the installed speaker wall.

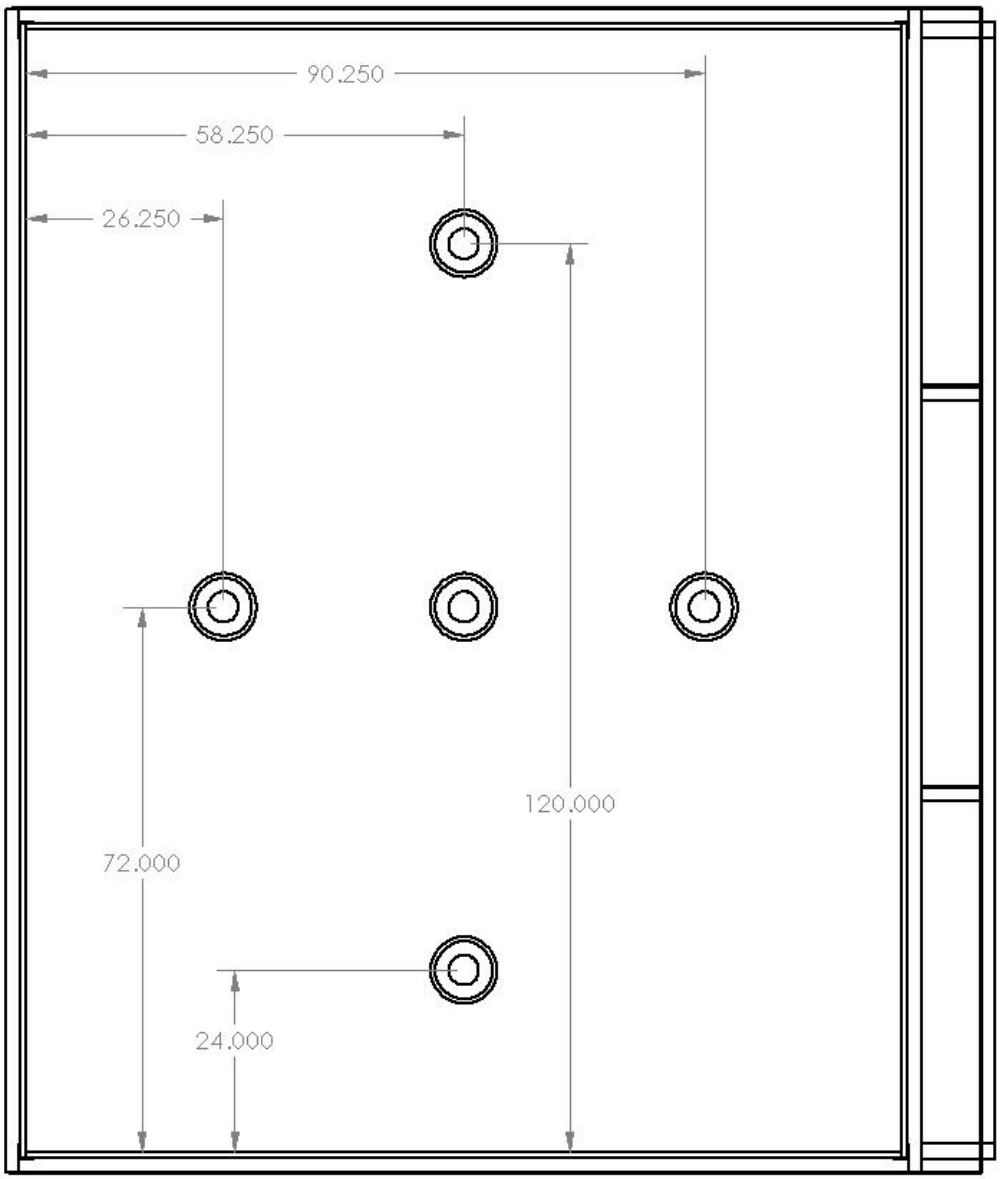

Figure 21. Placement of speakers on outside wall of corner four (view looking upstream, dimensions in inches)

Figure 22. Speaker wall viewed from inside (left) and outside (right) the KSWT

5.3 Amplitude of Acoustic Forcing in the Test Section

The speaker wall was tested with the tunnel turned on at 600 RPM. 600 RPM was chosen because the test section speed (approximately 17 m/s) is one of the highest test section speeds where frequencies below the planar cutoff of the test section can be tested. Three sound frequencies (45 Hz, 75 Hz, and 105 Hz) were tested; these frequencies were selected because they span the useable frequency range without coinciding with any motor or blade passing frequencies. The non-dimensional frequencies are 15.3×10^{-6} for 45 Hz, 25.6×10^{-6} for 75 Hz, and 35.6×10^{-6} for 105 Hz for these test conditions. Although these non-dimensional frequencies are small for a

standard receptivity experiment, they were chosen because they were below the planar cutoff frequency.

Figure 23, Figure 24 and Figure 25 show narrowband sound pressure level spectra during acoustic forcing at the three test frequencies. In all three cases, the peak in the spectrum created by acoustic forcing is larger than any of the nearby peaks caused by background noise. The first two harmonics of the forcing frequency are also present in the flow. In a typical receptivity experiment, measurements will be band-passed around the forcing frequency, so the harmonics do not directly affect the experiment; however, the harmonics will create disturbances that could affect the boundary layer basic state.

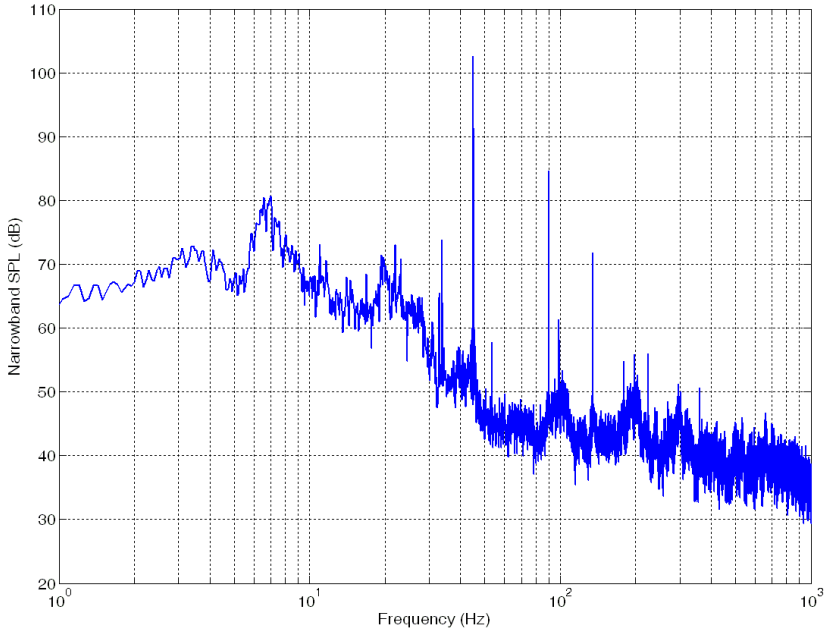

Figure 23. Test section narrowband SPL (600 RPM, 45 Hz, 0.88 V_{rms})

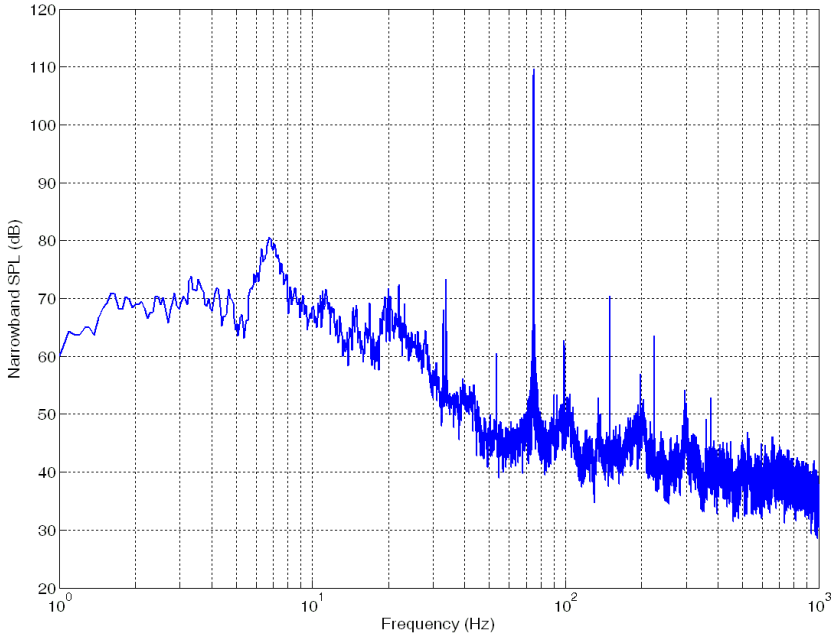

Figure 24. Test section narrowband SPL (600 RPM, 75 Hz, 0.88 Vrms)

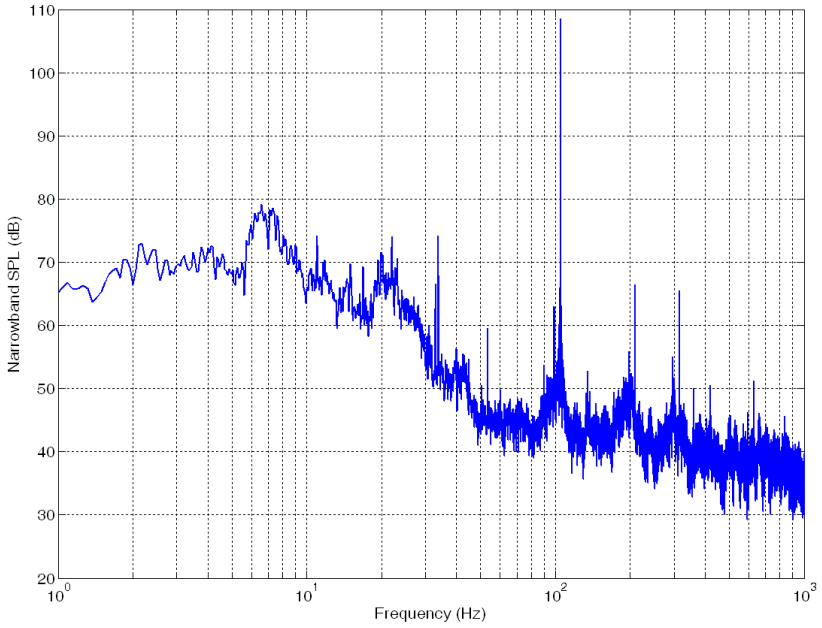

Figure 25. Test section narrowband SPL (600 RPM, 105 Hz, 0.88 Vrms)

Single direction sensing was used to decompose the acoustic forcing field into upstream and downstream traveling components. The microphones were narrow band passed around the forcing frequency, and the amplitude of the microphone signals was corrected for the decreased amplitude of the filter at the center frequency. The directional components of acoustic forcing are shown in Figure 26 on a linear scale and Figure 27 on a decibel scale.

Figure 26 and Figure 27 show that the amplitude of the upstream and downstream traveling waves depends on both forcing amplitude and frequency. The speakers were tested up to a 0.88 V_{rms}, which is lower than the 1.50 V_{rms} speaker power limit. At 0.88 V_{rms} input, the speaker wall produced over 105 dB of output in the test section; this amplitude is sufficient for most receptivity experiments. If larger amplitude sound is required, the forcing amplitude can be increased or more speakers can be added to the speaker wall.

The complex acoustics of the test leg of the KSWT also affects relative wave amplitudes. For example, forcing at 75 Hz created the strongest downstream traveling waves while forcing at 105 Hz created the strongest upstream traveling waves. The upstream traveling waves, which are created by the change in wind tunnel area downstream of the test section, appear to be very sensitive to the forcing frequency.

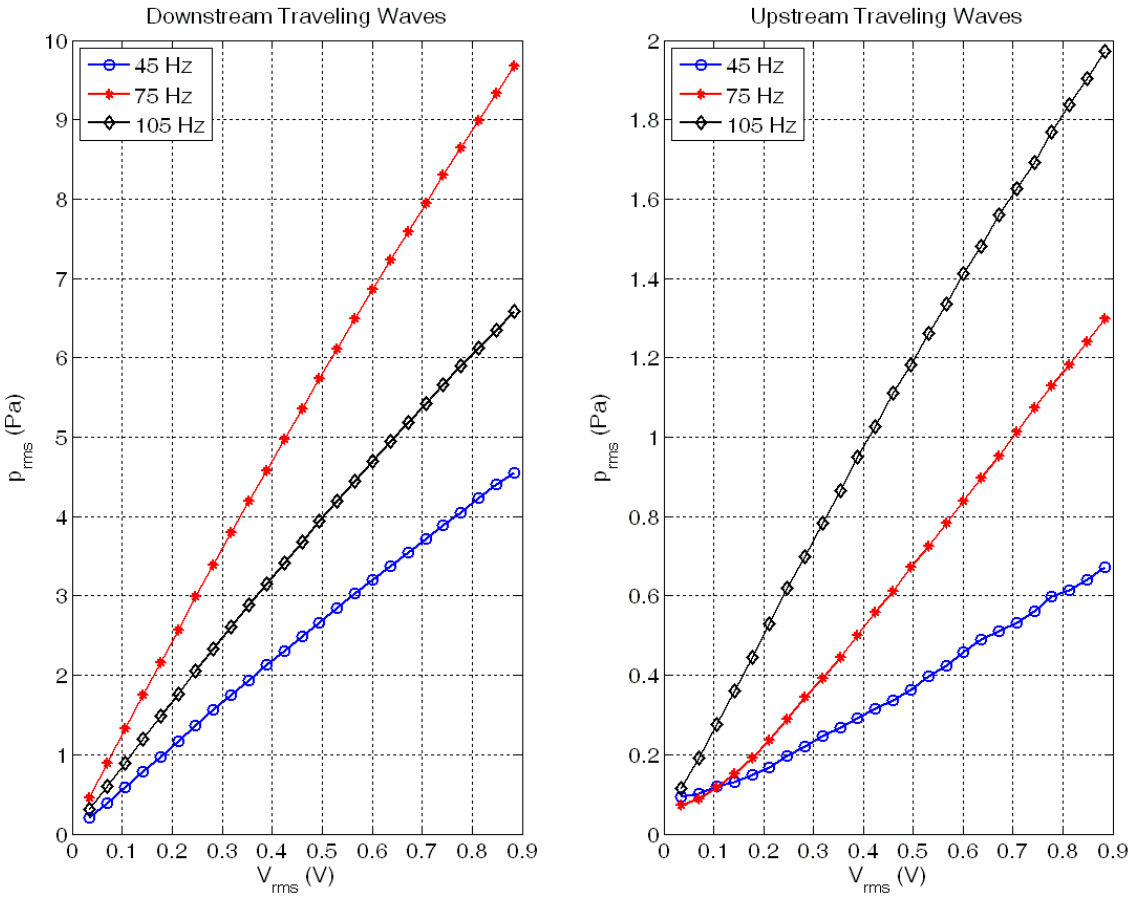

Figure 26. Comparison of downstream and upstream traveling waves created by acoustic forcing at 600 RPM

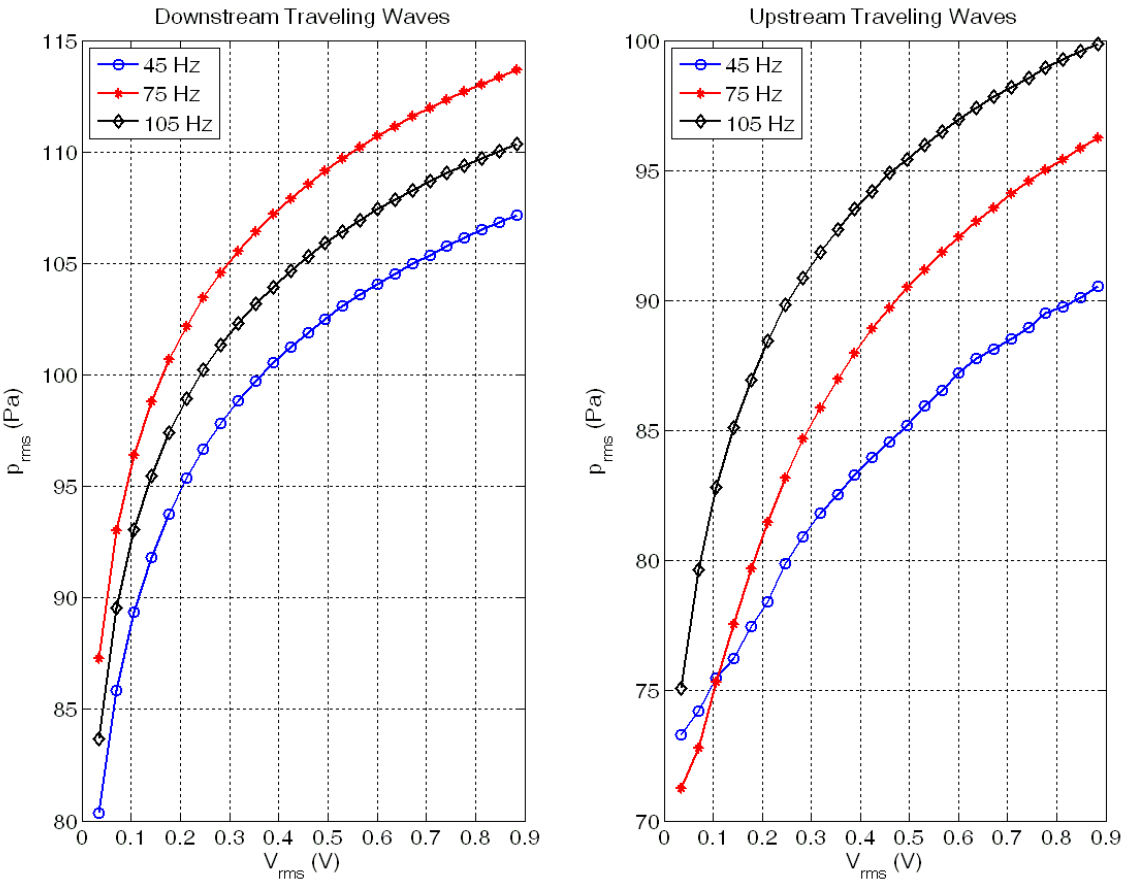

Figure 27. Comparison of downstream and upstream traveling waves created by acoustic forcing at 600 RPM (in dB)

Figure 28 shows the ratio of downstream traveling waves to upstream traveling waves during acoustic forcing. The ratio depends on both forcing frequency and amplitude. The ratio is a measure of the magnitude of reflected waves due to the diffuser; a high ratio means that the majority of sound energy is traveling downstream rather than oscillating in the test section due to a standing wave. The ratio is smallest at 105 Hz for4cing.

Wiegel and Wlezien (1993) decomposed the acoustic forcing field of the Arizona State Unsteady Wind Tunnel and found that a typical downstream to upstream ratio for the tunnel was 1.25. One of the major changes made to the KSWT when it was relocated to Texas A&M was a complete redesign of the diffuser downstream of the test section. The new diffuser design, which has a more gradual expansion gradient, reduces the amplitude of the reflected waves created during acoustic forcing. The downstream to upstream ratios in the KSWT range from 3 to 12 at moderate to high forcing values. Further reduction of the upstream traveling components will enhance acoustic receptivity experiments in the KSWT.

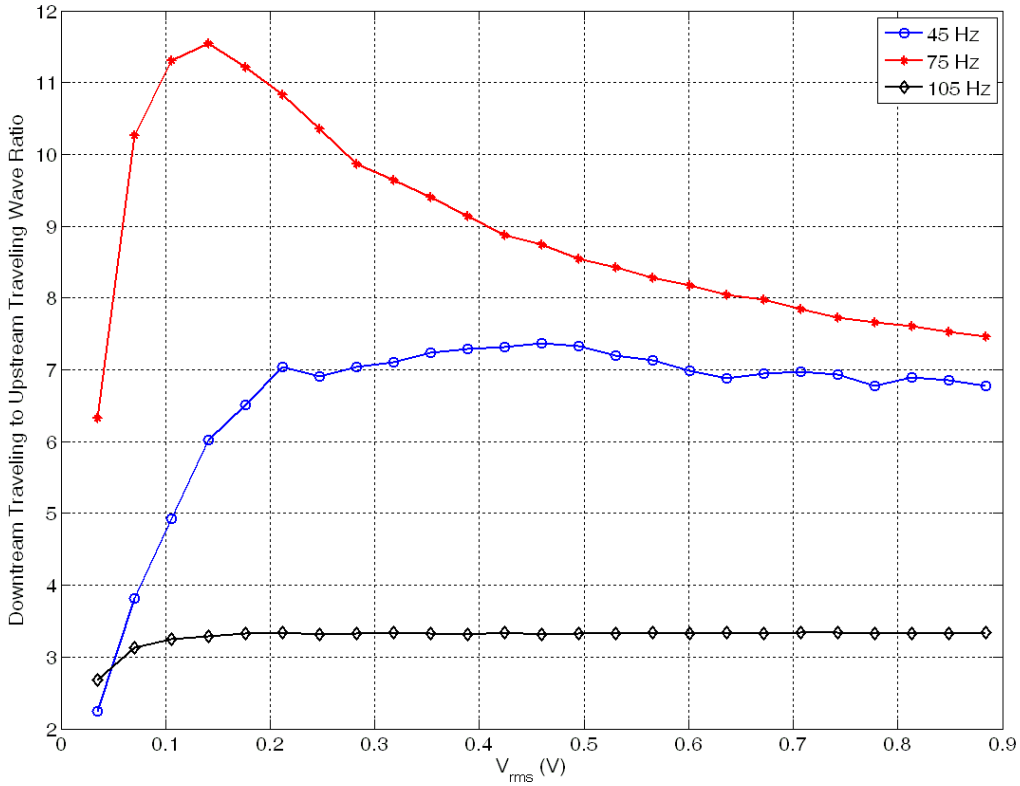

Figure 28. Ratio of downstream to upstream traveling waves for acoustic forcing at 600 RPM

6. CLOSED LOOP CONTROL OF ACOUSTIC REFLECTIONS

Section 5 described the installation of the speaker wall in the KSWT and documented the upstream and downstream traveling waves created in the test section during acoustic forcing. The diffuser reflections in the KSWT are smaller than the reflections measured in the Arizona State Unsteady Wind Tunnel due to the modified diffuser design, but further decreasing the amplitude of upstream traveling waves during acoustic forcing would enable more accurate acoustic receptivity studies.

Wiegel and Wlezien (1993) used secondary loudspeakers to cancel the reflected waves from acoustic forcing. Their experiment focused on non-localized receptivity and required a constant amplitude, downstream traveling acoustic field. The presence of the diffuser created a standing wave pattern that varied the amplitude of the forcing in the test section. They measured the amplitude and phase of the reflected waves and adjusted the amplitude and phase of the secondary speakers to cancel the upstream traveling waves.

An adaptive filtering technique for cancelling reflected waves is presented in this section. The adaptive technique is based off a linear, convolution filter and offers several advantages over the technique used by Wiegel and Wlezien. The technique was implemented successfully in the KSWT, and results are shown in this section.

6.1 The Need for an Adaptive, Time Domain Controller Approach

Initial active control attempts in the KSWT (Kuester & White 2010) were based on a broadband, frequency domain control scheme to eliminate tonal, upstream traveling

motor and fan noise. The control path - the acoustic path between the control speaker and the error sensor - was measured as part of the control scheme. The transfer function for the control path is shown in Figure 29. The transfer function was measured at 26 frequencies between 30 and 100 Hz as well as six different test section speeds between 0 m/s and 25 m/s. The frequency increases along each line, generally traveling clockwise around each loop.

The transfer function shows why frequency domain is not a viable control strategy for this application. Standing waves created by complex duct acoustics are present in the transfer function; these standing waves can be seen as interior loops on the complex plane as the frequency is increased. The standing waves create sudden changes in the transfer function phase that destabilize the control algorithm. Thus, the frequency domain technique is susceptible to complex duct acoustic effects and is not feasible for application in the KSWT.

Figure 29 also shows how changes in wind tunnel speed affect the control path transfer function. The large changes in the transfer function with different speeds makes a fixed amplitude & phase controller not ideal for this application. During a typical experiment in the KSWT, the wind tunnel speed is altered to maintain a constant Reynolds number at the test location. A fixed amplitude and phase controller is set by measuring both the primary reflection path and the control path and then setting the amplitude and phase of the control signal so upstream traveling waves in the test section are cancelled. The fixed controller will perform worse as the conditions of the experiment, and thus the transfer functions, change.

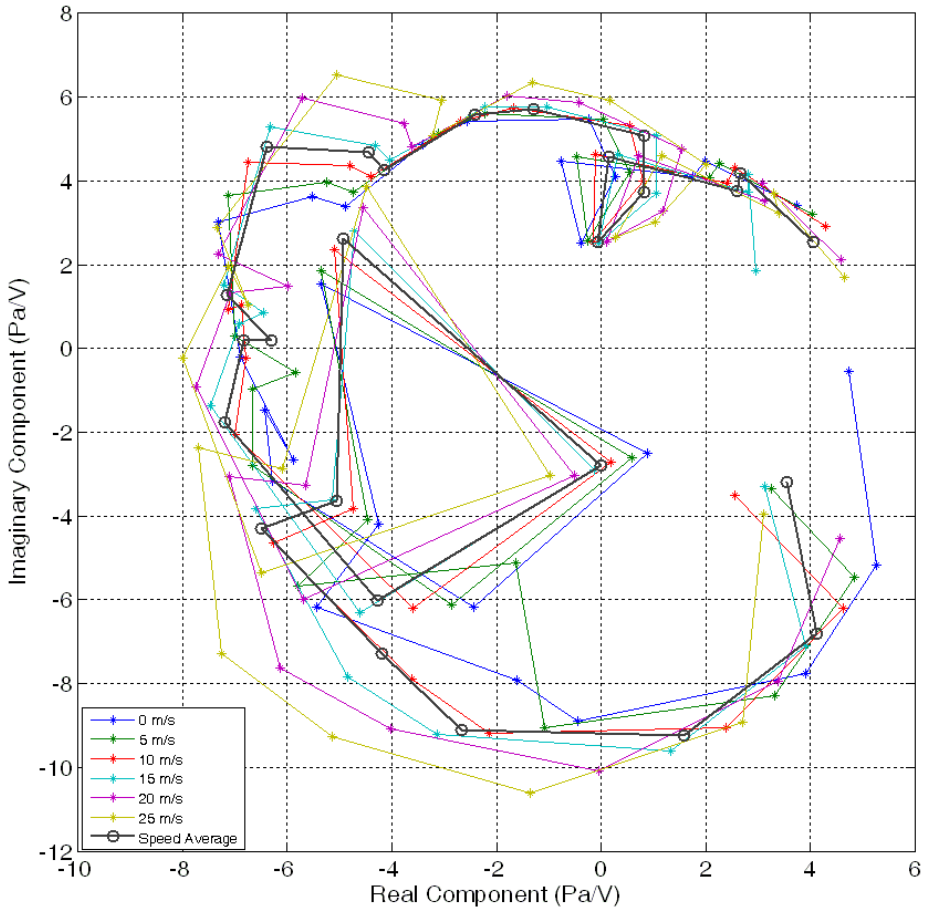

Figure 29. Control path transfer function in complex plane

If the control path has a strong dependence on frequency and freestream speed, the primary reflection path with also have also have strong dependencies on frequency and freestream speed. In addition, the air temperature inside of the tunnel also affects the transfer functions. An adaptive control system can continuously change during an experiment to minimize the upstream traveling waves, while a fixed controller may eliminate the upstream traveling waves to a lesser degree.

There are drawbacks to using an adaptive control system. Adaptive control systems require an error signal. The single-direction sensing technique described in Section 2 can be used as an error signal, but the two microphone technique does not perform well in signals with broad frequency, uncorrelated frequency content. The error signal also introduces a noise component to the control system. The error signal needs to be AC coupled and amplified to eliminate as much noise from the signal as possible.

6.2 Filtered-X Least Mean Squares Algorithm

The adaptive control technique used is the Filtered-X Least Mean Squares Algorithm (FXLMS). This algorithm is commonly used in active noise control applications. For this application, the signal sent to the primary subwoofers is used as a reference to remove the acoustic reflection created by the first stage diffuser. The algorithm utilizes a gradient descent technique to adapt a control filter to minimize the reflected waves. The error is measured by the single-direction sensing described in Section 2.

The control filter is a transverse, finite impulse response (FIR) filter. The output of the filter is dependent on both current and past inputs. Equation (11) shows the definition of the output of a transverse filter of length L; n is the time index, $y(n)$ is the filter output, $w_l(n)$ are the weight coefficients at time index n, and x is the input signal.

$$y(n) = \sum_{l=0}^{L-1} w_l(n)x(n-l) = \boldsymbol{w^T(n)x(n)} \tag{11}$$

The adaptive filter adjusts the weights in Equation (11) such that the mean squared error is minimized. Kuo and Morgan (1996) prove that, for statistically

stationary signals, the mean squared error has a global minimum at a certain set of weight coefficients. The mean square error, defined by the different permutations of N weight coefficients, is a parabolic surface in N dimensions. Utilizing these facts, the weights in the filter are updated so they move along the negative gradient of the error surface. The weight update equation is shown in Equation (12).

$$\boldsymbol{w}(n+1) = \boldsymbol{w}(n) - \mu\nabla\xi(n) \tag{12}$$

where μ is a constant, called the convergence coefficient, that controls how far to move down the gradient surface and ξ is the mean square error. In most cases, the mean square error is estimated using the squared instantaneous error signal.

$$\xi(n) = e^2(n) \tag{13}$$

Substituting Equation (13) into Equation (12) yields the weight update for the FXLMS algorithm.

$$\boldsymbol{w}(n+1) = \boldsymbol{w}(n) - 2\mu[\nabla e(n)]e(n) \tag{14}$$

The implementation of the FXLMS algorithm for this application is shown in Figure 30. A forcing signal drives the speaker wall located in corner four of the KSWT; the sound from the speaker wall travels downstream and is reflected by the diffuser. Meanwhile, the forcing signal is filtered by the controller, and the output is sent to a secondary loudspeaker. The sound from the secondary speaker travels upstream and destructively interferes with the reflected sound. Figure 31 shows the primary acoustic path and the control path in relation to the test leg of the KSWT.

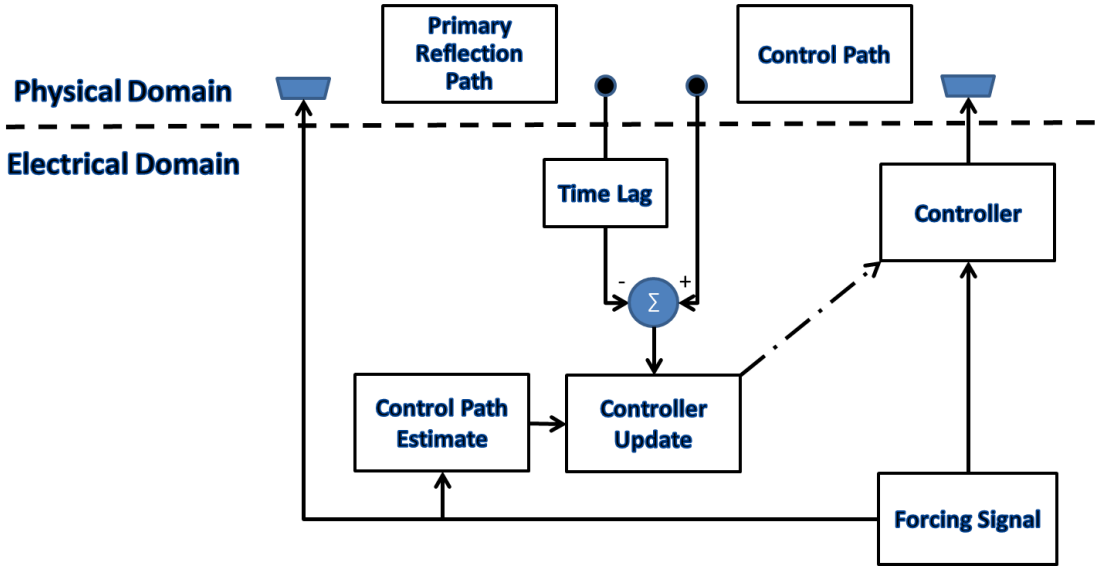

Figure 30. Adaptive control flow chart

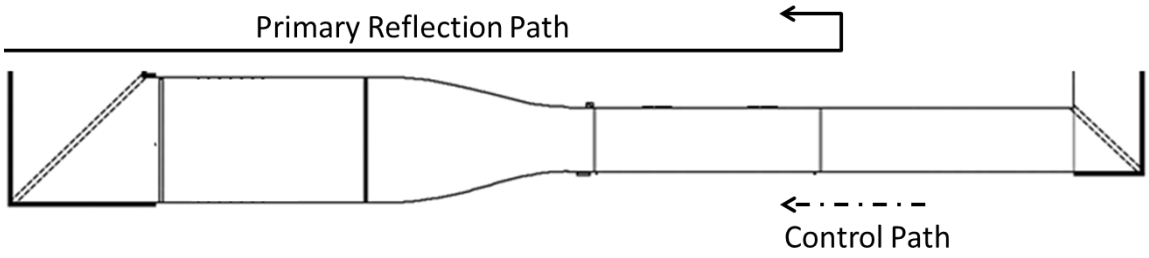

Figure 31. Primary reflection acoustic path and control path

The time domain, single-direction sensing technique described in Section 2 will provide the error signal. The single-direction sensing output (*e(n)*) will measure both the primary reflection (*d(n)*) and the output of the control system. The measured error is shown in Equation (15) where *s(n)* is the control path and *y(n)* is the output from the control speaker.

$$e(n) = d(n) + \boldsymbol{s}(n) * y(n) = d(n) + \boldsymbol{s}(n) * [\boldsymbol{w}^T(n)\boldsymbol{x}(n)] \quad (15)$$

Taking the gradient of the instantaneous error with respect to the weight vector results in

$$\nabla e(n) = \boldsymbol{s}(n) * \boldsymbol{x}(n) \tag{16}$$

Substituting Equation (16) into Equation (14) gives the weight update equation for the algorithm.

$$\boldsymbol{w}(n+1) = \boldsymbol{w}(n) - 2\mu[\boldsymbol{s}(n) * \boldsymbol{x}(n)]e(n) \tag{17}$$

The algorithm is called filtered-x least mean squares because the input must be convolved by the secondary path to update the filter weights. In order for the algorithm to function, the secondary (or control) path must be estimated. Kuo and Morgan (1996) describe an offline estimation technique that was adapted for use in this application and shown in Figure 32. A known forcing signal is sent through the secondary loudspeaker, and the upstream traveling waves are measured by the error sensors. The FIR estimate of the control path is used to filter the forcing signal, and the filtered output is compared to the microphone measurement to create an error signal. This error signal is used to update the control path estimate through the following equation

$$\boldsymbol{s}(n+1) = s(n) + 2\mu_s \boldsymbol{x}(n)\big(e(n) - \boldsymbol{s}^{\boldsymbol{T}}(n)\boldsymbol{x}(n)\big) \tag{18}$$

The secondary path should be estimated at the operating point (temperature, wind tunnel speed) that the experiment will be performed. Kuo and Morgan (1996) show that the FXLMS algorithm will converge as long as the phase of the secondary path estimate is within 90^{o} of the actual secondary path. The known forcing can either be a linear chirp signal that spans the frequency range of interest or a sine wave at the forcing frequency.

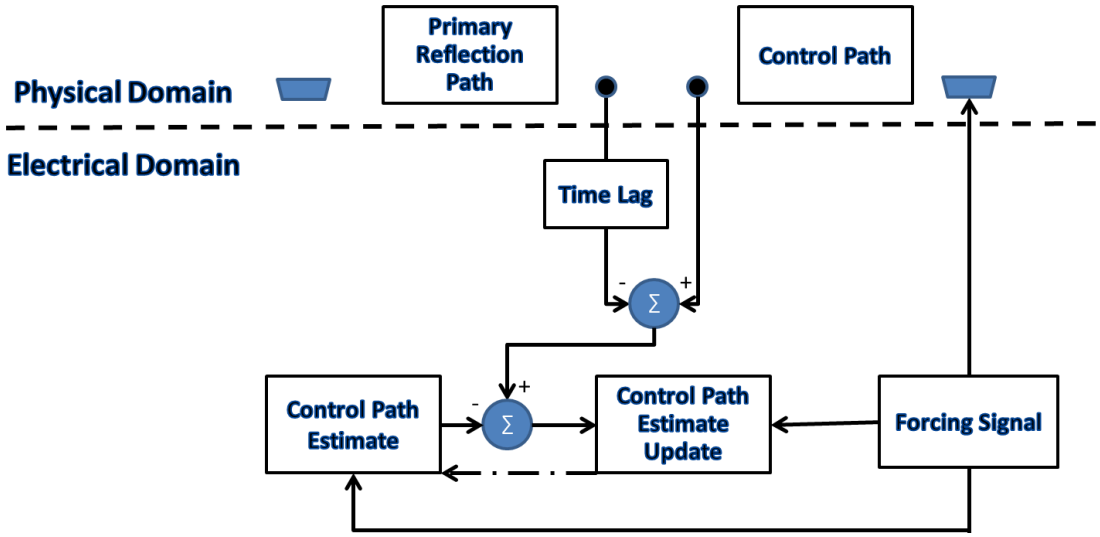

Figure 32. Offline control path estimate flow chart

Several parameters affect the performance of the FXLMS algorithm. The sampling frequency must be large enough to capture all of the frequencies of interest and small enough that all of the necessary calculations can be performed each cycle iteration. The filter length must be long enough to capture the lowest frequency of interest but short enough to limit the computation time of each loop iteration. The convergence coefficient affects the stability of the algorithm; if the convergence coefficient is too large, the filter weights will diverge rather than stabilize. If the convergence coefficient is too small, the filter weights will converge slowly and be susceptible to noise. The optimum convergence coefficient depends on both the filter length and the magnitude of the error signal. All three of these parameters should be adjusted to optimize the performance of the control algorithm.

6.3 Control System Hardware and Software

The microphone hardware used for the error sensor is the same hardware used for all acoustic measurements in the KSWT. The error microphones were filtered and amplified by a Stewart/Kemo VBF44 analog filter. The control output was filtered by an Alligator Technologies USBPGF-S1A programmable low-pass filter. A National Instruments CompactDaq (Model 9178) system was used for data acquisition. Two National Instruments cDaq 9215 modules with BNC connectors provide ± 10 V range with 16 bit resolution, while a National Instruments cDaq 9263 module provides the digital to analog conversion for the control output.

The control speaker is a McCauley 6222 10 inch diameter subwoofer, the same speaker model that was installed on the speaker wall. The speaker control signal is amplified by a factor of 23 through an ADCOM GFA 555-II amplifier. In order to not overload the 300 W continuous power capacity of the speakers, the input to the amplifiers should be held under 1.50 V_{rms}. In practice, this is accomplished by limiting the maximum output amplitude the 1.80 V.

The control system and offline control path estimate are controlled through in house National Instruments LabView VIs. Screenshots of the control panel for each program are shown in Figure 33.

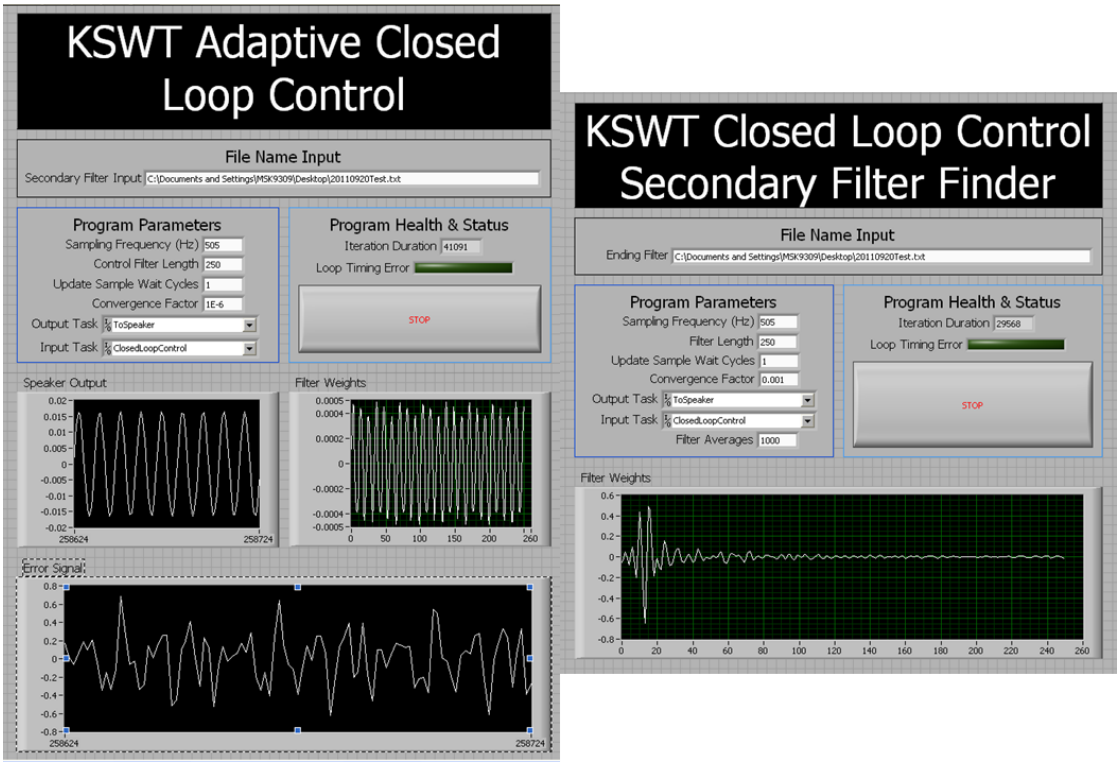

Figure 33. Screenshots of closed loop control and secondary filter finder command windows

The error sensor microphones were placed 27.0 inches (0.686 meters) apart at the downstream end of the test section; this separation corresponded to a sampling frequency between 500 Hz and 508 Hz depending on the air temperature in the tunnel. The filter length was set to 250; this set the time scale of the filter to ~ 0.5 seconds. The convergence coefficient was set to $1x10^{-3}$ for offline control path estimation and $1x10^{-6}$ during operation. These values were selected through operational experience.

6.4 Effectiveness of Control System

Active control was attempted at the same test points used during speaker wall testing in Section 4. Three different frequencies (45 Hz, 75 Hz, and 105 Hz) were tested

with the tunnel running at 600 RPM. Two microphones, placed at locations one and two as denoted by Table 1, decomposed the sound field in the test section into upstream and downstream traveling components.

The effect of the control system at 45 Hz is shown in Figure 34. Active control successfully reduced the amplitude of upstream traveling waves in the test section. At low amplitude forcing, the error sensors are more susceptible to noise, and thus the control system is not effective. As the forcing amplitude was increased, the control system decreased the upstream traveling wave amplitude.

In addition to the decrease in the amplitude of upstream traveling waves, the control system had a negligible effect on the amplitude of the downstream traveling waves. The ability to alter the upstream traveling waves while keeping the downstream traveling wave amplitude constant allows the effects of the wave direction to be studied through comparisons of measurements with and without the control system.

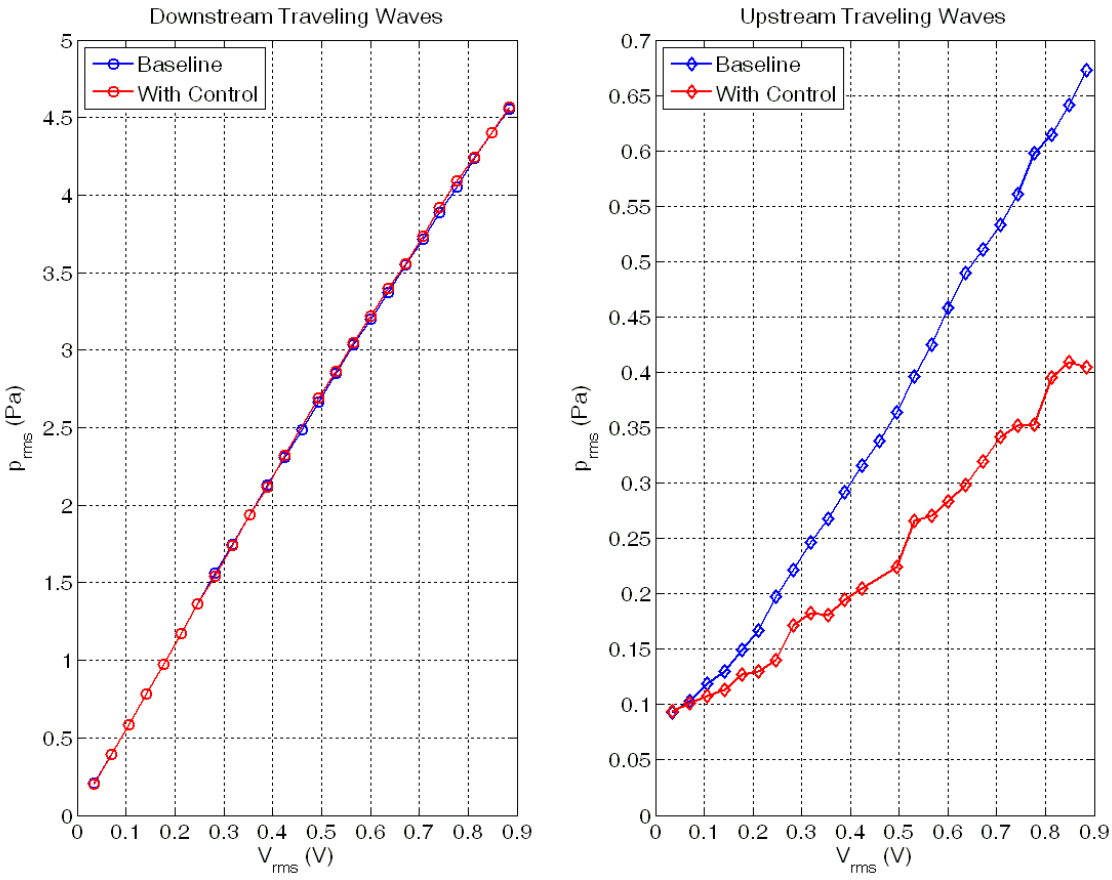

Figure 34. Effect of active control system on upstream and downstream traveling waves at 600 RPM and forcing frequency 45 Hz

The effect of active control for 75 Hz forcing is shown in Figure 35. At 75 Hz, the control system is not very effective. The downstream waves are not strongly affected, but the upstream traveling wave amplitude increased for most of the test points. At larger forcing amplitudes, the upstream traveling wave amplitude is decreased slightly.

The reason for the failure of the control system at 75 Hz is not entirely clear. With the wind tunnel turned off (0 RPM), upstream traveling waves were successfully

cancelled; thus, the role of tunnel speed coupled with the complex acoustics of the test leg is partially responsible for the poor performance. Further optimization of error sensor placement could increase the effectiveness of the control system at this frequency.

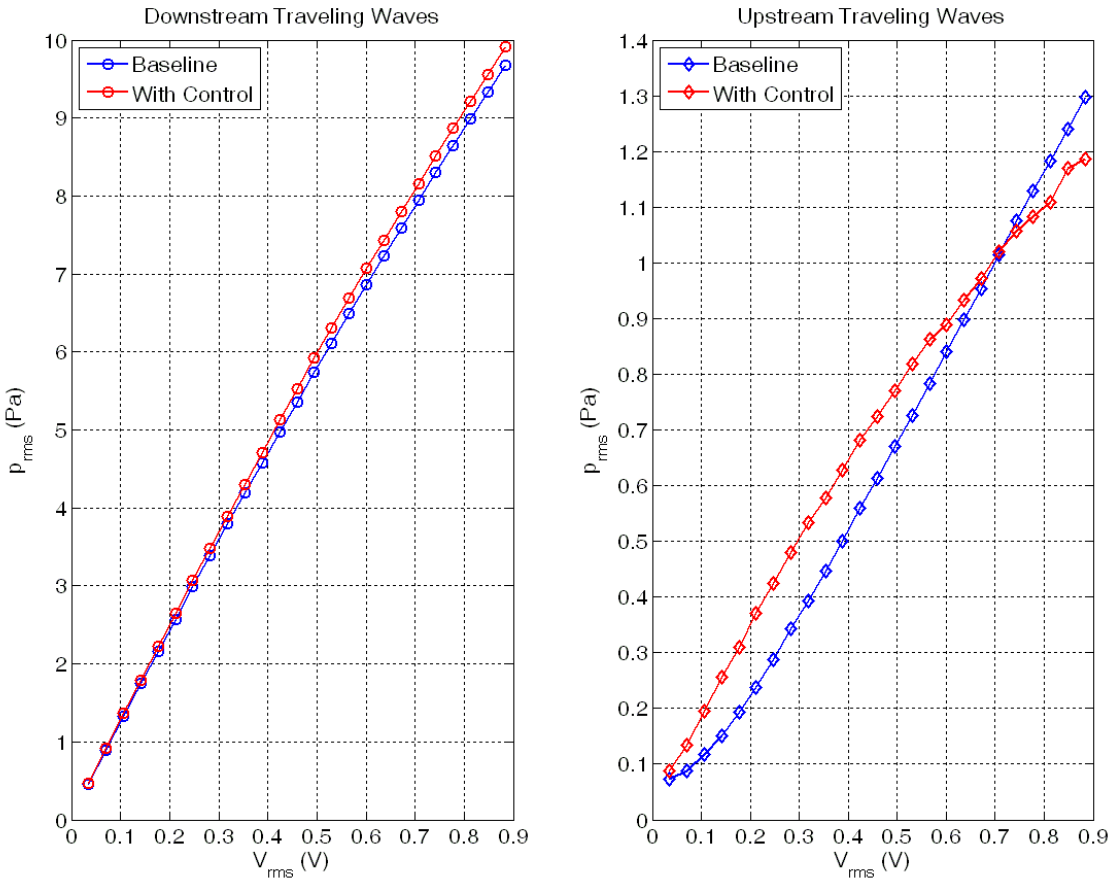

Figure 35. Effect of active control system on upstream and downstream traveling waves at 600 RPM and forcing frequency 75 Hz

The effect of active control for 105 Hz forcing is shown in Figure 36. The upstream traveling component is decreased significantly while the downstream traveling component varies less than 1% from the baseline value. Without control, the 105 Hz

reflection was larger than the 45 Hz and 75 Hz reflections. With control, the 105 Hz reflection is reduced up to 88% from the baseline value.

Active control was successful up to 0.74 V_{rms} forcing; at this amplitude, the control speaker reached its maximum power output which caused the control program to shut down. The control program can be modified to keep the speaker at the maximum output when the controller creates a signal that exceeds the speaker power requirement, but the ideal solution is to add control power by installing another subwoofer. The additional speaker could be installed next to the current speaker, or it could be installed in a different location in the first stage diffuser. The first option would involve minimal changes to the control system; the control power would be doubled by sending the same control signal to both loudspeakers. The second option potentially offers more control efficiency; the two speakers can work in harmony to compensate for complex duct acoustic effects. For example, if one speaker is placed at the node of a standing wave, the other speaker can still effectively cancel the upstream traveling waves. Each speaker would have its own control path estimate filter and control filter. The two controllers would run simultaneously and send signals to each loudspeaker that cancel the upstream traveling waves.

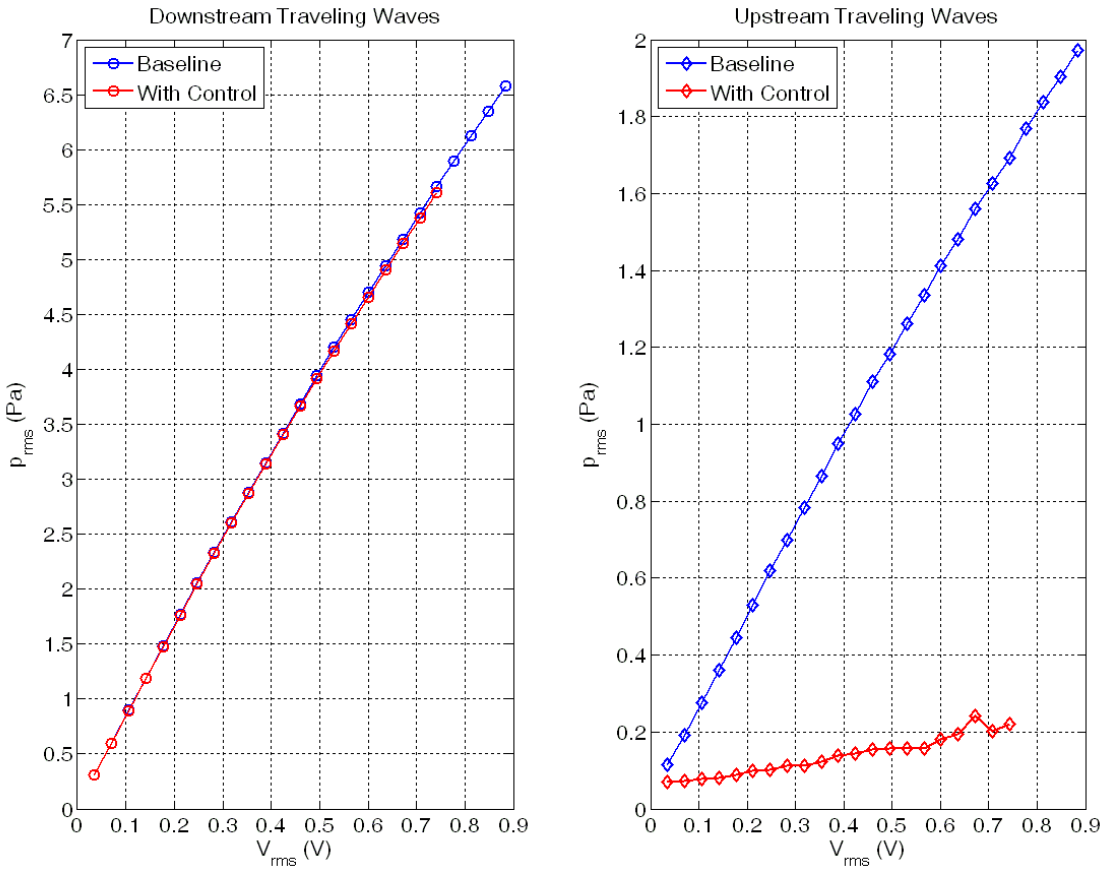

Figure 36. Effect of active control system on upstream and downstream traveling waves at 600 RPM and forcing frequency 105 Hz

Finally, the downstream to upstream traveling wave ratio is shown in Figure 37. The potential of the adaptive technique can be seen in how the control system affects the ratio at 105 Hz forcing. Wiegel and Wlezien (1993) reported a downstream to upstream traveling wave ratio of 12 with their fixed controller. With the adaptive controller activated, the downstream to upstream traveling wave ratio at 105 Hz goes as high as 28.

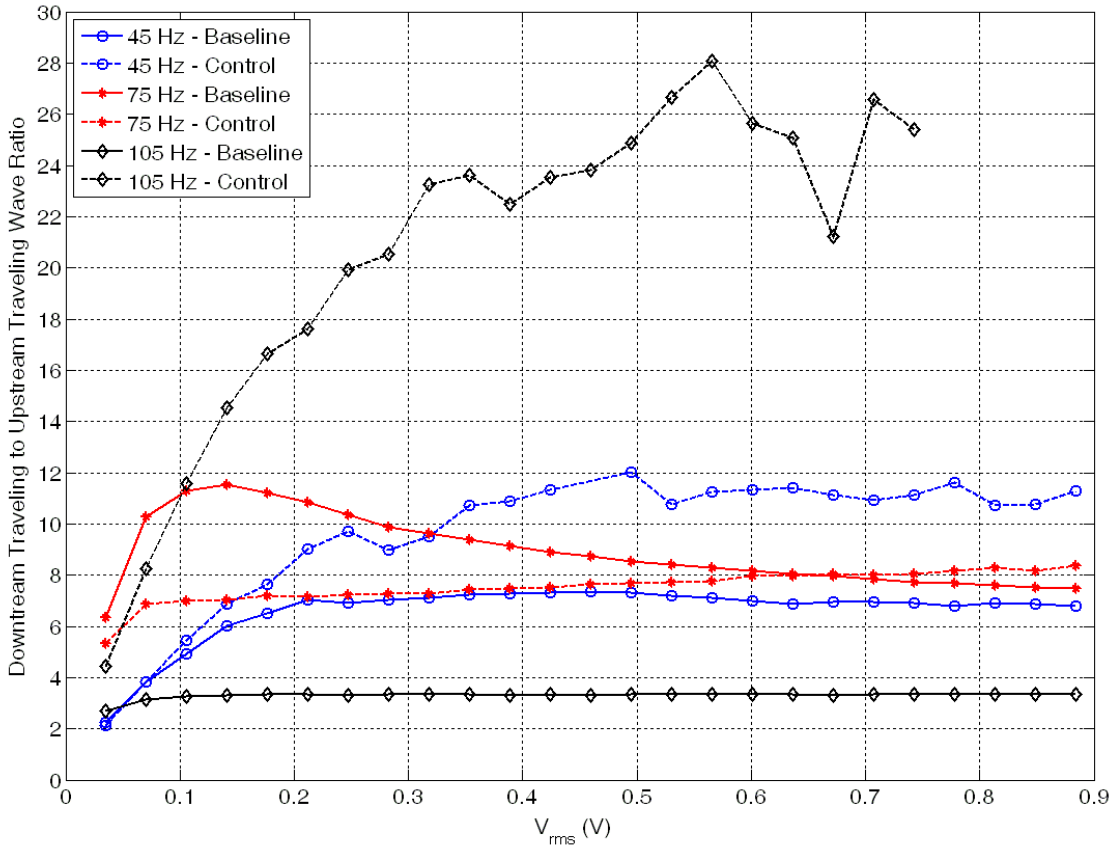

Figure 37. Ratio of downstream to upstream traveling waves for acoustic forcing at 600 RPM, with and without active control

The preceding results show that active control of acoustic reflections using an adaptive controller has potential to improve acoustic receptivity experiments. Further optimization of error sensor location and control speaker location may improve the performance of the algorithm at certain frequencies, but the adaptive capabilities of the system offer several advantages over a fixed control technique.

7. CONCLUSIONS

This thesis documents the acoustics of the KSWT in preparation for future sound receptivity experiments. Measurements of the background noise levels in the KSWT show that the majority of pressure fluctuations in the tunnel are low frequency (less than 30 Hz) and originate from two locations: the corner one/corner two transition and the extended diffuser. These low-frequency oscillations are undesirable but do not directly affect experiments. At frequencies higher than 30 Hz, tonal noise from the motor and the fan are distinguishable from a low broadband, background noise level. Directional separation of waves in the test section revealed that motor and blade passing noise primarily travels upstream into the test section.

To determine the effect of interior acoustic treatments on background noise levels, the foam and broadband acoustic panels inside of the tunnel were covered using 5 mm thick plywood to create an acoustically rigid surface. Microphone measurements showed that the acoustic treatments located in corner one have only a small effect of the tunnel background noise, while the treatments in the plenum remove tonal and broadband noise. The addition of acoustic treatments in corner one and corner two may further improve the background noise levels in the test section.

Five speakers were installed in the plenum to create downstream traveling sound. The sound output from the speakers was measured in the test section for three test frequencies. Spectrum measurements during acoustic forcing showed that the background noise levels in the KSWT were low enough to allow acoustic forcing to be

the predominant flow feature. The acoustics of the test leg of the KSWT makes the sound field frequency dependent. In particular, upstream traveling reflections created by changes in wind tunnel area have a large frequency dependence. The reflections are smaller in the KSWT than in the ASU Unsteady Wind Tunnel due to alterations in the diffuser downstream of the test section.

An adaptive, closed loop control system was implemented to eliminate the upstream traveling reflections created during acoustic forcing. The adaptive technique offers advantages over a fixed controller scheme used by Wiegel and Wlezien (1993). The input signal used to drive the primary subwoofers is multiplied by a transverse filter; the output from the filter is then used to a control a secondary loudspeaker that creates an upstream traveling wave which in turn destructively interferes with the reflections. The controller removed the reflections with varying degrees of success depending on the forcing frequency. At 105 Hz, the controller reduced the magnitude of upstream traveling wave significantly and created downstream to upstream traveling ratios greater than 20. Further refinement of the control system, including error sensor and control speaker placement, will improve the performance of the control system.

REFERENCES

Crouch JD (1992a) Non-localized receptivity of boundary layers. J Fluid Mech. 244:567-581

Crouch JD (1992b) Localized receptivity of boundary layers. Phys. Fluids A:4(7)1408-1414.

Duell E, Walter J, Arnette S, Yen J (2002) Recent advances in large-scale aeroacoustic wind tunnels. 8th AIAA/CEAS aeroacoustics conference, paper, 2002-2503.

Fuciarelli D, Reed HL, Lyttle I (2000) Direct numerical simulation of leading-edge receptivity to sound. AIAA J. 38(7):1161-1164

Goldstein, ME (1983) The evolution of Tollmien–Schlichting waves near a leading edge. J Fluid Mech. 127:59-81

Haddad OM, Erturk E, Corke TC (2005) Acoustic receptivity of the boundary layer over parabolic bodies at angles of attack. J Fluid Mech. 536:377-400

Hammerton PW, Kerschen EJ (1996) Boundary-layer receptivity for a parabolic leading edge. J Fluid Mech. 310:243-267

Heinrich RA, Kerschen EJ (1989) Leading-edge boundary-layer receptivity to freestream disturbance structures. J. Appl. Math. Mech. (ZAMM) 69(6):T596-T598

Hunt LE, Downs RS, Kuester MS, White EB, Saric WS (2010) Flow quality measurements in the Klebanoff–Saric Wind Tunnel. 27th AIAA aerodynamic measurement technology and ground testing conference, paper, 2010-4538

Hunt LE, Saric WS (2011) Boundary-layer receptivity of three-dimensional roughness arrays on a swept wing. 41st AIAA fluid dynamics conference, paper, 2011-3881

Kendall JM (1991) Studies on laminar boundary-layer receptivity to freestream turbulence near a leading edge. in Boundary Layer Stability and Transition to Turbulence, ASME Technical Report FED 114:23-30

Kerschen EJ (1990) Boundary layer receptivity theory. Appl. Mech. Rev. 43(5-2):152-157

Krutckoff, TK (1996) Experiments on boundary-layer receptivity to sound. Thesis, Arizona State University.

Kuester, MS, White, EB (2010) Implementation of active noise control in a closed-circuit wind tunnel. Online Bulletin of the APS http://meetings.aps.org/link/BAPS.2010.DFD.LJ.4. Accessed 3 January 2012.

Kuo SM, Morgan DR (1996) Active noise control systems: algorithms and DSP implementations. Wiley, New York, pp 1-88

Morkovin MV, Reshotko E, Herbert T. (1994) Transition in open flow systems — a reassessment. Bulletin of the APS. 39(9):1882

Nishioka M, Morkovin, MV (1986) Boundary-layer receptivity to unsteady pressure gradients: experiments and overview. J Fluid Mech. 171:219-261

Press WH, Teukolsky SA, Vetterling WT, Flannery BP (2007) Numerical recipes: the art of scientific computing, 3rd edition. Cambridge, New York, pp 603-717

Saric WS, Reed, HL, Kerschen (1994) Leading edge receptivity to sound: experiments, DNS, and theory. 25th AIAA fluid dynamics conference, paper, 1994-2222

Saric WS, Wei W, Rasmussen BK, Krutckoff TK (1995) Experiments on leading-edge receptivity to sound. 36th AIAA fluid dynamics conference, paper, 1995-2253

Saric WS, Reshotko E (1998) Review of flow quality issues in wind tunnel testing. 29th AIAA fluid dynamics conference, paper, 1998-2613

Saric WS, White EB (1998) Influence of high-amplitude noise on boundary-layer transition to turbulence. 29th AIAA fluid dynamics conference, paper, 1998-2645

Saric WS, White EB, Reed HL (1999) Boundary-layer receptivity to freestream disturbances and its role in transition (invited). 30th AIAA fluid dynamics conference, paper, 1999-3788

Welch, PD (1967) The use of fast Fourier transforms for the estimation of power spectra: a method based on time averaging over short, modified periodograms. IEEE Transactions on Audio Electroacoustics, AU-15:70-73

Wiegel M, Wlezien, RW (1993) Acoustic receptivity of laminar boundary layers over wavy walls. AIAA shear flow conference, paper, 1993-3280

White EB, Saric WS, Radeztsky RH (2000) Leading-edge acoustic receptivity measurements using a pulsed-sound technique. in Laminar-Turbulent Transition, Springer, New York, pp. 103-108

VITA

Name:	Matthew Scott Kuester
Address:	Klebanoff–Saric Wind Tunnel Texas A&M University 1771 George Bush Drive West College Station, TX 77845-4762
Email Address:	matt.kuester@gmail.com
Education:	B.S., Aerospace Engineering, Texas A&M University M.S., Aerospace Engineering, Texas A&M University